






Remodelling of the endothelial extracellular matrix promotes smooth muscle cell hyperplasia in pulmonary hypertension due to left heart disease

Netra Nambiar Veetil^{1,2,3,4}, Tara Gransar^{1,2,3}, Shao-Fei Liu^{1,4}, Ahed Almalla⁵, Marieluise Kirchner⁶, Robyn Brackin-Helmers⁷, Felix Hennig^{2,3}, Ruhi Yeter^{2,3}, Marie Weinhart^{5,8}, Philipp Mertins⁶, Volkmar Falk ^{2,3,4,9}, Robert Szulcek ^{1,3,4,10,11}, Mariya M. Kucherenko ^{1,2,3,4,*†}, Wolfgang M. Kuebler ^{1,4,11,12,13†}, and Christoph Knosalla ^{2,3,4†}

¹Institute of Physiology, Charité—Universitätsmedizin Berlin, Corporate Member of Freie Universität Berlin and Humboldt-Universität zu Berlin, Charitéplatz 1, Berlin 10117, Germany;

²Department of Cardiothoracic and Vascular Surgery, Deutsches Herzzentrum der Charité, Augustenburger Platz 1, Berlin 13353, Germany; ³Charité—Universitätsmedizin Berlin, Corporate Member of Freie Universität Berlin and Humboldt-Universität zu Berlin, Charitéplatz 1, Berlin 10117, Germany; ⁴DZHK (German Centre for Cardiovascular Research), Partner Site Berlin, Berlin, Germany; ⁵Institute of Chemistry and Biochemistry, Freie Universität Berlin, Takustr. 3, Berlin 14195, Germany; ⁶Core Unit Proteomics, Berlin Institute of Health at Charité—Universitätsmedizin Berlin and Max-Delbrück-Center for Molecular Medicine, Berlin 13125, Germany; ⁷Advanced Medical Bioimaging Core Facility, Charité—Universitätsmedizin Berlin, Charitéplatz 1, Berlin 10117, Germany; ⁸Institute of Physical Chemistry and Electrochemistry, Leibniz Universität Hannover, Callinstr. 3A, Hannover 30167, Germany; ⁹Department of Health Science and Technology, Translational Cardiovascular Technology, LFW C 13.2, ETH Zurich, Universitätstrasse 2, Zürich 8092, Switzerland; ¹⁰Department of Cardiac Anesthesiology and Intensive Care Medicine, Deutsches Herzzentrum der Charité, Augustenburger Platz 1, Berlin 13353, Germany; ¹¹DZL (German Centre for Lung Research), Partner Site Berlin, Berlin, Germany; ¹²Departments of Physiology, University of Toronto, 1 King's College Circle, Toronto, ON M5S 1A8, Canada; and ¹³Department of Surgery, University of Toronto, 1 King's College Circle, Toronto, ON M5S 1A8, Canada

Received 21 January 2025; revised 10 June 2025; accepted 17 September 2025; online publish-ahead-of-print 3 December 2025

Time of primary review: 76 days

Aims

Hyperplasia of pulmonary arterial smooth muscle cells (SMCs) contributes to the progression of pulmonary hypertension (PH), yet the underlying pathomechanism of this process in PH secondary to left heart disease (PH-LHD) is poorly understood. We aimed to investigate the role of the endothelial extracellular matrix (ECM), specifically the pulmonary arterial basement membrane (BM), in influencing SMC proliferation and phenotypic changes in PH-LHD.

Methods and results

SMC hyperplasia and endothelial ECM remodelling were characterized histologically on human pulmonary arterial samples, and by mass spectrometry, and atomic force microscopy on decellularized ECM (dECM) produced *in vitro* by endothelial cells isolated from pulmonary arteries (PA) of LHD patients without pulmonary hypertension (LHD w/o PH), PH-LHD patients, or healthy-heart controls. Proliferation and migration rates of SMC cultured on endothelial dECM were assessed by Ki67 immunostaining and by wound-healing assay, respectively. The role of mechanosensitive YAP1 in SMC hyperplasia was addressed in human cells and in an aortic-banding rat model of PH-LHD by analysing YAP1 activation and the effect of YAP1 inhibition. PA of LHD w/o PH and PH-LHD patients showed extensive remodelling of the BM. This was confirmed *in vitro* as altered composition and stiffening of dECM generated by respective patient endothelial cells. ECM remodelling was associated with SMC accumulation in the pulmonary arterial intima in patient samples and promoted SMC migration and proliferation *in vitro*. Conversely, dECM generated by healthy human endothelial cells reduced the hypermigration and hyperproliferation of SMC from LHD w/o PH and PH-LHD patients. Remodelling of the endothelial ECM in LHD w/o PH and PH-LHD patients also activated YAP1 in SMC, inhibition of which reduced SMC migration and proliferation *in vitro*. These findings were reproduced *in vivo* in a rat model of PH-LHD induced by aortic-banding.

* Corresponding author. Tel: +49 30 450 528 535; fax: +49 30 450 528 920, mariya.kucherenko@charite.de

† These authors share the last authorship.

© The Author(s) 2025. Published by Oxford University Press on behalf of the European Society of Cardiology.

This is an Open Access article distributed under the terms of the Creative Commons Attribution-NonCommercial License (<https://creativecommons.org/licenses/by-nc/4.0/>), which permits non-commercial re-use, distribution, and reproduction in any medium, provided the original work is properly cited. For commercial re-use, please contact reprints@oup.com for reprints and translation rights for reprints. All other permissions can be obtained through our RightsLink service via the Permissions link on the article page on our site—for further information please contact journals.permissions@oup.com.

Conclusion

Here, we report endothelial ECM remodelling as a key mechanism driving SMC hyperplasia in PH-LHD. Notably, endothelial ECM remodelling is evident in both patients with LHD w/o PH and those with PH-LHD, raising the possibility that it may reflect an early event in LHD-induced pulmonary vascular remodelling. This ECM remodelling is associated with YAP1 in adjacent SMC, promoting their migration and proliferation and contributing to SMC hyperplasia. Consequently, targeting ECM remodelling and YAP1 activation may offer promising therapeutic strategies for preventing of PA remodelling in PH-LHD.

Keywords

Pulmonary hypertension • Left heart disease • Endothelial ECM • YAP1 • Smooth muscle cell hyperplasia

1. Introduction

Up to 10% of the adult population is affected by left heart disease (LHD).^{1,2} Progressive left heart failure with increased end-diastolic pressure and increased left atrial filling pressure results in pulmonary hypertension (PH) by a passive transmission of elevated pressures into pulmonary veins, capillaries, and arteries.³ The increase of pressure triggers remodelling and stiffening of both pulmonary arteries (PA) and pulmonary veins, contributing to an additional rise in pulmonary vascular resistance (PVR), which marks the transition from isolated post-capillary pulmonary hypertension (IpcPH) to combined post- and pre-capillary pulmonary hypertension (CpcPH).⁴ In LHD patients, PH significantly increases morbidity and mortality by increasing the hemodynamic load on the right ventricle (RV), first by leading to adaptive hypertrophy followed by dilatation and ultimately failure.⁵ Among the five groups of PH classified by the World Health Organization (WHO), PH secondary to left heart disease (PH-LHD) is by far the most common³ but as well the least studied. At present both an in-depth pathomechanistic understanding as well as approved therapeutic strategies are lacking.

Smooth muscle cell (SMC) hyperplasia represents a hallmark of pulmonary vascular remodelling in pulmonary arterial hypertension (PAH).^{6–8} Hyperproliferation and hypertrophy of resident SMCs have been proposed to drive SMC hyperplasia, resulting in occlusive pulmonary vascular remodelling.^{6,7,9} From small PAs and arterioles, SMCs migrate further into the distal lung vasculature, leading to vessel muscularization, stiffening, and occlusion.^{10,11} In proximal PAs, SMC hyperplasia is particularly prominent in the intimal region and contributes to vessel stiffening by increased deposition of fibrillar collagens into the arterial wall.¹² While in the systemic vasculature, intimal SMC hyperplasia has been linked to endothelial injury,^{13,14} elastic fibre degradation,¹⁵ and vascular inflammation,¹⁶ the triggers and signalling pathways driving SMC hyperplasia in the pulmonary arterial conduit vessels, i.e. the pulmonary arterial trunk and the main left and right PAs, are poorly understood.

A growing body of evidence implicates extracellular matrix (ECM) remodelling, including basement membrane (BM) remodelling, as a significant factor in the pathogenesis of PH.^{8,17–25} PA ECM remodelling in both PAH and PH-LHD is characterized by an increased expression and crosslinking of fibrillar collagens and as such promotes vascular stiffening.^{20,23,26,27} The vascular BM represents a thin layer of specialized ECM, which is mainly produced and maintained by endothelial cells (ECs) and consists of non-fibrillar network-forming collagen IV (COL4), laminins (LAM), and dynamic components, such as fibronectin, proteoglycans, perlecan, and nidogens.²⁴ This physiological composition of the BM is crucial for maintaining the homeostasis of the arterial wall in that, for example, BM LAMs limit the transmigration of immune cells into the arterial media^{28–32} while COL4 regulates EC adhesion and barrier function.²⁵ Consequently, pathological remodelling of the BM has been associated with a range of systemic vasculopathies, including diabetes³³ and arteriosclerosis.³⁴ Yet, its relevance to the pathology of PH has only recently emerged. Specifically, several studies in PAH have linked BM remodelling to a dysfunction of PA ECs, resulting in a dysbalanced production of COL4 and LAM.^{8,35}

As a transcriptional co-activator of the Hippo signalling pathway, yes-associated protein 1 (YAP1), has recently become implicated in the pathobiology of PAH due to its ability to convert extracellular mechanical cues

into intracellular signals—a process called mechanotransduction. Under homeostatic conditions, YAP1 nuclear activity is suppressed through its phosphorylation at serine 127 by the large tumour suppressor kinases 1 and 2 (LATS1/2), resulting in its cytoplasmic retention.³⁶ Changes in ECM stiffness or composition are sensed by focal adhesion complexes containing collagen-binding integrins which in turn activate intracellular signalling cascades involving focal adhesion kinase and SRC tyrosine kinases.^{36–38} These pathways then drive YAP1 nuclear translocation through both Hippo-dependent and -independent mechanisms³⁶ leading to the expression of YAP1 target genes that enhance cell survival and motility.^{36–40} An alternative mechanism of YAP1 activation in a stiff matrix environment involves the modulation of nuclear envelope mechanics, driven by increased cytoskeletal tension through the assembly of actin stress fibres and engagement of linker of nucleoskeleton and cytoskeleton (LINC) complexes.^{41,42} The resulting mechanical forces promote nuclear flattening which increases nuclear pore permeability thus facilitating the passive import of YAP1.^{42,43} As such, activated YAP1 can regulate the proliferation and migration of pulmonary vascular cells in response to changes in ECM composition²⁵ and/or stiffness.^{8,23,44}

In the present study, we report BM remodelling in PAs of patients with left heart disease without PH (LHD w/o PH) and left heart disease with PH (PH-LHD). In LHD w/o PH patients, the endothelial ECM was significantly stiffer than in healthy-heart donors, and this effect was even more pronounced in PH-LHD patients. Concurrently, we identified SMC hyperplasia in the intimal layer that was evident in patients with LHD w/o PH and further exacerbated in PH-LHD. *In vitro*, SMCs isolated from both patient groups showed increased migration and proliferation rates. Exploration of the mechanistic link between ECM remodelling and SMC hyperplasia revealed that communication from the remodelled endothelial ECM to SMCs involves activation of the mechanosensitive transcriptional co-activator YAP1 as a driver of SMC migration and proliferation. Consistent with this mechanism, YAP1 inhibition reduced hypermigration and hyperproliferation of human SMCs from LHD patients *in vitro*. Analogously, *in vivo* administration of a YAP1 inhibitor attenuated SMC migration and proliferation in a preclinical rat model of PH-LHD.

2. Methods

Pulmonary trunk specimens (hereafter referred to as PA) of LHD w/o PH patients ($n = 25$), PH-LHD patients ($n = 31$), and healthy-heart donors (control, $n = 14$) were collected during orthotopic heart transplantation (at the Deutsches Herzzentrum der Charité) when the length of the PA was adjusted before anastomosis. PH was defined according to current guidelines as a mean pulmonary arterial pressure (mPAP) higher than 20 mmHg at rest³ (Table 1). The collection of biomaterials was approved by the Ethics Committee of the Charité-University Medicine Berlin (EA4/035/18, EA1/134/23) with informed consent of the patients. The study was conducted in accordance with the principles of the Declaration of Helsinki. Information on patients' age, sex, underlying disease, as well as data obtained by right heart catheterization within 6 months before heart transplantation was retrieved from clinical records. Different patient samples were used in different assays, and individual n -numbers for each assay are given in the respective figure legend. Pulmonary trunk specimens obtained from a rat model of PH-LHD after

Table 1 Clinical patient characteristics

Clinical variables	Control (n = 14)	LHD w/o PH (n = 25)	PH-LHD (n = 31)
Sex			
Female (%)	6 (42)	11 (44)	11 (36)
Male (%)	8 (58)	14 (56)	20 (64)
Age (years)			
Median	36.6	52.0	57.0
Mean \pm SD	39.1 \pm 14.4	50.2 \pm 11.8	54.9 \pm 10.3
Range	45	39	48
Body weight (kg)	80.4 \pm 15.3	87.1 \pm 19.2	79.1 \pm 20.9
Height (cm)	175.9 \pm 8.6	174.1 \pm 7.8	176.0 \pm 11.0
Underlying diseases (%)			
ICM	–	32	22
NICM	–	8	12
DCM	–	48	48
HCM	–	4	9
Danon disease	–	4	–
Cardiac sarcoidosis	–	4	–
Myocarditis	–	–	9
Haemodynamics, Mean \pm SD			
mPAP (mmHg)	–	14.7 \pm 4.4	33.7 \pm 9.5
Cardiac output (l/min)	–	4.4 \pm 1.1	3.8 \pm 1.3
Cardiac index (l/min/m ²)	–	2.4 \pm 0.9	2.3 \pm 1.1
PVR (dynes·sec·cm ⁻⁵)	–	110.2 \pm 79.3	316.2 \pm 245.9
TPG (mmHg)	–	5.5 \pm 3.0	12.9 \pm 6.8

ICM, ischaemic cardiomyopathy; NICM, non-ischaemic cardiomyopathy; DCM, dilated cardiomyopathy; HCM, hypertrophic cardiomyopathy; mPAP, mean pulmonary arterial pressure; PVR, pulmonary vascular resistance; TPG, transpulmonary gradient.

aortic-banding (AoB)^{45,46} were reprocessed from the study by Liu et al.⁴⁷ Animal studies were performed in accordance with the recommendations of the Federation of European Laboratory Animal Science Association, the guidelines from Directive 2010/63/EU of the European Parliament on the protection of animals used for scientific purposes and approved by the local government authorities (LAGeSo; animal protocols nos. G0030/18). In short, for the study, male Sprague-Dawley rats (80–100 g) underwent supracoronary aortic banding (AoB) to induce PH-LHD. Rats were anaesthetized with intraperitoneally administered ketamine (87 mg/kg bw) and xylazine (13 mg/kg bw), intubated, and mechanically ventilated. A titanium clip was placed on the ascending aorta to restrict blood flow, while sham-operated rats underwent the same procedure without the aortic clamping. All animals received preoperative analgesia with 5 mg/kg bw carprofen administered intraperitoneally and postoperative analgesia with 5 mg/kg bw per day carprofen administered intraperitoneally for 1 week. Post-surgery, rats received analgesia and antibiotics. After 4 weeks, rats were treated with either verteporfin (VP) or vehicle for 6 weeks. Echocardiography and hemodynamic assessments were performed, followed by euthanasia under deep anaesthesia by exsanguination and tissue collection for further analysis.⁴⁷ In this study, only male rats were included due to model-related differences in PH-LHD progression between sexes that are driven by substantial differences in growth rate—males exhibit up to 40% greater body weight compared to females by week 5 post-AoB. This disparity leads to more pronounced aortic constriction and, consequently, a stronger disease phenotype in males that is evident as early as 3 weeks post-AoB.^{27,47} In contrast, females develop a milder phenotype, with increased right ventricular systolic pressure observed at 5 weeks post-AoB, and PA stiffening and right RV hypertrophy becoming apparent only at 9 weeks post-AoB, thus preventing pharmacological

testing within the established 3–9 week time window in this model in females.⁴⁸

All methods are further detailed in the [supplement Methods](#).

3. Results

3.1 PAs of PH-LHD patients show SMC hyperplasia and BM remodelling

Analysis of human PA samples identified hyperplasia of smooth muscle actin-positive (SMA⁺) SMCs in LHD w/o PH and more so in PH-LHD patients that resulted in progressive widening of the PA intimal region relative to controls (Figure 1A–D, for patient characteristics, see Table 1, and Materials and Methods). This intimal SMC layer contained accumulated collagen fibres, as detected by SHG imaging (Figure 1E), which may potentially contribute to the increased PA wall stiffness in PH-LHD recently reported by us.²⁷ Intimal width correlated positively with pulmonary hemodynamic parameters, namely mPAP, pulmonary capillary wedge pressure (PCWP), and PVR (Figure 1F and G), highlighting the potential relevance of SMC hyperplasia in the pathogenesis of PH-LHD.

To probe for the potential mechanisms of SMC hyperplasia, we assessed migration and proliferation rates in primary SMCs isolated from patient and donor PAs *in vitro*. Wound-healing assay experiments and staining for the cell proliferation marker Ki67 followed by quantification of Ki67-positive (Ki67⁺) cells, showed that SMCs from both LHD w/o PH and PH-LHD patients exhibited increased migration, and SMCs from PH-LHD patients also exhibited increased proliferation compared to control SMCs (Figure 1H–H'; [Supplementary material online, Figure S1A–B](#)). Given the recognized role of the ECM in regulating these cell functions,¹⁸ we assessed the relation between SMCs and the endothelial BM in PA samples from control subjects, LHD w/o PH, and PH-LHD patients by co-immunostaining for the SMC marker SMA and the BM marker COL4. Plot line analysis identified a clear separation of COL4 peak intensity and SMA⁺ SMCs in control samples; however, both signals colocalized in LHD w/o PH and PH-LHD samples (Figure 1I and I'), indicating an accumulation of SMCs in the BM.

Based on these results, we hypothesized that LHD may cause remodelling of the endothelial BM, which in turn promotes SMC hyperproliferation and migration via ECM-to-cell signalling, ultimately causing SMC hyperplasia in PH-LHD (Figure 1J).

3.2 Endothelial BM is remodelled in PAs of LHD w/o PH and PH-LHD patients

Transmission electron microscopy (TEM) of PA samples from control subjects shows the endothelial BM as a condensed thin structure underneath the ECs. In contrast, in LHD w/o PH patients, the BM-like material was disorganized and widened, while in PH-LHD samples it appeared largely degraded (Figure 2A–A'). Evaluation of the BM markers COL4 and LAM showed widened signals in LHD w/o PH yet a diminished BM in PH-LHD samples (Figure 2B–E). Plot line analysis showed reduced COL4 and LAM peak intensity in both LHD w/o PH and PH-LHD PAs compared to control PAs (Figure 2F and G), suggesting a loosened BM structure with degradation of BM components.

To obtain a better understanding of the associated compositional and biomechanical changes in the BM, which is formed *in vivo* by the adjacent ECs, we generated and examined decellularized ECM (dECM) produced by primary ECs isolated from the PAs of control subjects, LHD w/o PH, or PH-LHD patients. Basal COL4 deposition by cultured ECs and efficient ECM decellularization were validated as described in the supplement (see [Supplementary material online, Video, Supplementary material online, Figure S2A](#)). Assessment of mechanical properties by atomic force microscopy (AFM) revealed a stiffness of 379 \pm 291 Pa in dECM generated by control ECs, which increased significantly in LHD w/o PH (516 \pm 400 Pa) and was highest in PH-LHD dECM (827 \pm 319 Pa) (Figure 2H). This stiffening correlated with elevated type I collagen expression in EC lysates, as

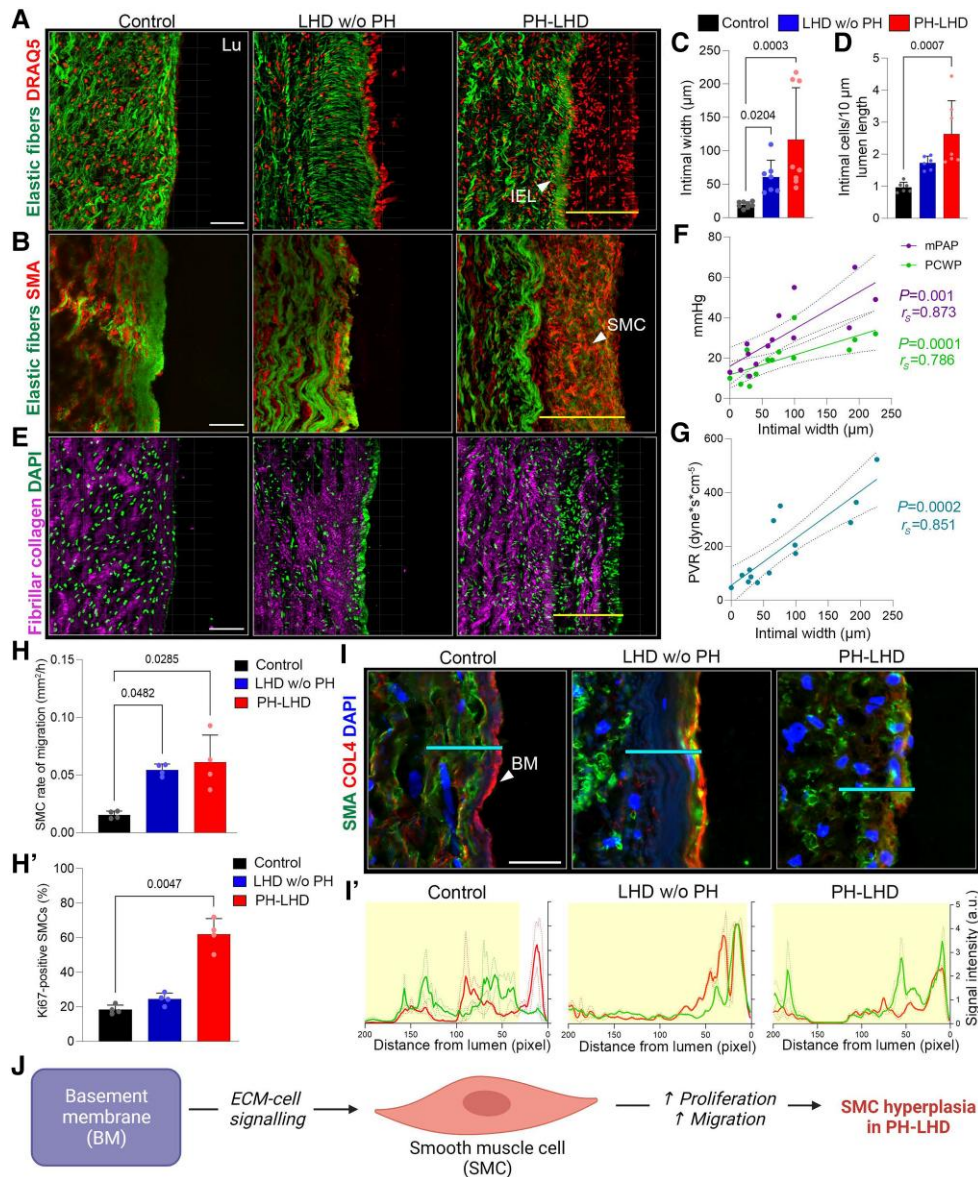


Figure 1 In PH-LHD, SMC hyperplasia is evident in PAs. **A**, Representative confocal microscopic images of PAs from control subjects or LHD w/o PH and PH-LHD patients with elastic fibres detected by autofluorescence in green; cell nuclei are visualized by DRAQ5 staining. In PH-LHD, note the extra cell layer apically of the inner elastic lamina (IEL) in the intima (marked by the yellow line). Lu, vessel lumen. **B**, Representative confocal microscopic images of PAs with elastic fibres (autofluorescence in green) and SMCs (immunostaining against α -smooth muscle actin; SMA). Note that the extra cell layer apically of the IEL (marked by the yellow line) in PH-LHD contains SMCs. **C**, Bar graph (mean \pm SD) with individual data points shows intimal width in PAs from control subjects ($n = 8$) or LHD w/o PH ($n = 7$) and PH-LHD ($n = 8$) patients. **D**, Bar graph (mean \pm SD) with individual data points shows number of cells within the intimal layer normalized to lumen surface length in PAs from control subjects ($n = 6$) or LHD w/o PH ($n = 6$) and PH-LHD ($n = 7$) patients. **E**, Representative confocal microscopic images of PAs from control subjects or LHD w/o PH and PH-LHD patients with fibrillar collagens detected by second harmonic generation (SHG) imaging and nuclei are visualized by DAPI staining. Note that the extra SMC layer apically of the IEL (marked by the yellow line) deposits fibre-forming collagens in PH-LHD. **F**, Spearman correlation analysis shows association between PA intimal width and mean pulmonary arterial pressure (mPAP), or pulmonary capillary wedge pressure (PCWP) as assessed by right heart catheterization in $n = 14$ LHD patients. **G**, Spearman correlation analysis shows association between PA intimal width and pulmonary vascular resistance (PVR) as assessed by right heart catheterization in $n = 14$ LHD patients. **H-H'**, Bar graphs (mean \pm SD) with individual data points show migration (wound-healing assay) and proliferation (Ki67 immunostaining) rate of primary SMCs isolated from PAs of control subjects ($n = 4$) and LHD w/o PH ($n = 4$) or PH-LHD ($n = 4$) patients cultured on 0.1% gelatin. **I**, Representative confocal microscopic images of PAs from control subjects and LHD w/o PH or PH-LHD patients immunostained for the SMC marker SMA or the BM marker collagen 4 (COL4); nuclei are visualized by DAPI staining. **I'**, Line graphs show averaged SMA and COL4 signal intensities along a straight line (cyan) perpendicular to the lumen surface ($n = 6$ biologically independent PA samples per group); a.u., arbitrary units. **J**, Schematic depicts proposed mechanism of SMC hyperplasia in PH-LHD, with BM remodelling promoting SMC migration and proliferation via ECM-to-cell signalling ultimately resulting in SMC hyperplasia and PA remodelling in PH-LHD. Scale bars are 50 μ m in **A**, **B**, **E**, and 40 μ m in **I**. Statistics: Two-tailed Mann–Whitney U test (**C–D**, **H**) and two-tailed Spearman correlation (**F**, **G**); corresponding P -values for statistical significance and r -values for correlation coefficient are given.

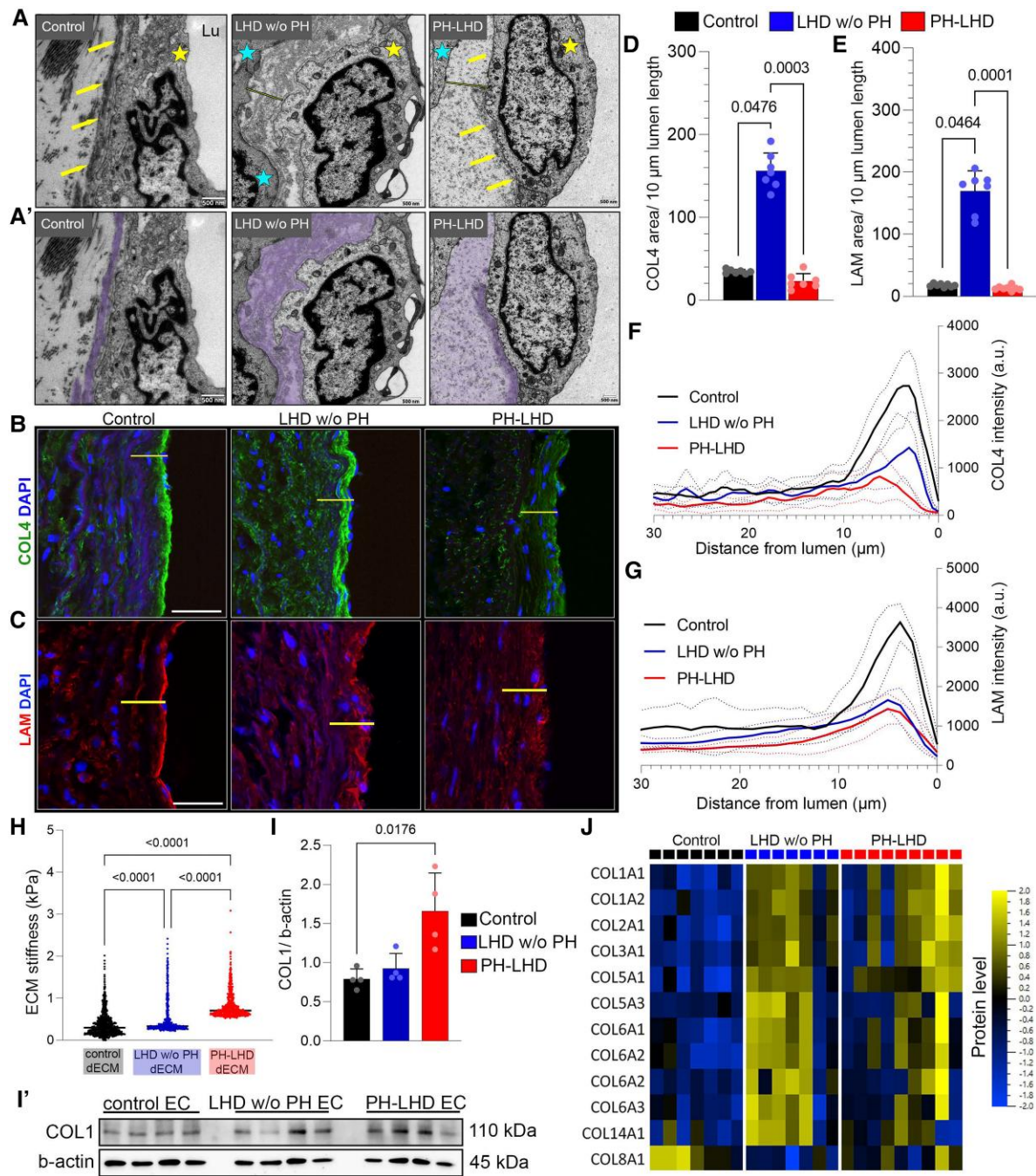


Figure 2 In LHD, BM remodelling precedes the development of PH. A-A', Representative electron microscopic images show endothelial BM in PAs from controls subjects and LHD w/o PH or PH-LHD patients with BM marked by yellow arrows in A and by purple shading in A', and ECs and SMCs marked by yellow and cyan stars, respectively. Note the widening of the BM-like material in LHD w/o PH and its loosening in PH-LHD. B and C, Representative confocal microscopic images of PAs immunostained for the BM marker COL4 (B) or LAM (C); nuclei are visualized by DAPI staining. D and E, Bar graphs (mean + SD) with individual data points show intimal COL4 and LAM positive area normalized to lumen surface length in PAs of control subjects ($n = 7$ for COL4, $n = 8$ for LAM) or LHD w/o PH ($n = 7$ for COL4 and LAM) and PH-LHD ($n = 7$ for COL4, $n = 8$ for LAM) patients. F and G, Line graphs show averaged COL4 and LAM signal intensities along a straight line (yellow in B and C) perpendicular to the lumen surface in PAs of control subjects ($n = 6$ for COL4, $n = 8$ for LAM) and LHD w/o PH ($n = 5$ for COL4, $n = 7$ for LAM) or PH-LHD ($n = 8$ for COL4 and LAM) patients. H, Dot plot shows Young's modulus of the decellularized endothelial extracellular matrix (dECM) produced by ECs isolated from PAs of control subjects ($n = 4$) and LHD w/o PH ($n = 4$) or PH-LHD ($n = 4$) patients as measured by AFM. I, Bar graph (mean + SD) with individual data points shows densitometric quantification of COL4 protein levels (normalized to β -actin) in ECs isolated from PAs of control subjects ($n = 4$) and LHD w/o PH ($n = 4$) or PH-LHD ($n = 4$) patients as assessed by western blotting; corresponding blots in I'. J, Heat map shows relative protein expression levels for differentially regulated collagens in dECM produced by EC isolated from PAs of control subjects ($n = 7$) and LHD w/o PH ($n = 7$) or PH-LHD ($n = 9$) patients as determined by mass spectrometry. Scale bars are 500 μ m in A and A', and 40 μ m in B and C. Statistics: Kruskal-Wallis test with Dunn's correction for multiple comparisons (D, E, H, and I); P-values for statistical significance are given.

shown by western blotting (Figure 2I–I'; Supplementary material online, Figure S3). Mass spectrometric analyses of dECM generated *in vitro* further revealed increased abundance of fibrillar collagens (COL1, COL2, COL3, and COL5), fibril-associated collagens (COL12 and COL14), and network-forming collagen COL6 in both LHD w/o PH and PH-LHD compared to control ECs, with a most pronounced increase observed in the LHD w/o PH group (Figure 2J). These findings suggest that LHD w/o PH is associated with substantial changes in ECM composition, yet matrix stiffening is even more pronounced in PH-LHD, presumably due to additional factors beyond ECM protein abundance such as increased crosslinking of fibrils that collectively enhance mechanical resistance.

3.3 Remodelled endothelial ECM promotes SMC migration and proliferation in LHD

Based on the finding of a remodelled endothelial-derived ECM, we next probed its potential functional role on PA SMC migration and proliferation. To this end, we cultured PA SMCs obtained from control, LHD w/o PH, or PH-LHD patients on dECM produced by either control, LHD w/o PH, or PH-LHD ECs, and assessed migration and proliferation by a wound-healing assay and immunostaining for the cell proliferation marker Ki67 (Figure 3A).

Relative to baseline migration rates of PA SMCs on gelatin coating, dECM produced by LHD w/o PH or PH-LHD ECs, but not dECM produced by control ECs, increased the migration of control SMCs. In SMCs of LHD w/o PH or PH-LHD patients, however, dECM produced by LHD w/o PH or PH-LHD ECs had no similar amplifying effect (Figure 3B and C). Rather, culturing LHD w/o PH or PH-LHD SMCs on an dECM produced by control ECs decreased their migration relative to baseline (Figure 3C). The latter effect was associated with a decrease in focal adhesions and cytoskeletal tension (see Supplementary material online, Figure S4) both of which are essential for cell migration.^{49–52} These results support the hypothesis that the remodelled endothelial ECM in LHD w/o PH or PH-LHD promotes migration of control SMCs and show conversely that an ECM produced by control ECs may reduce the migration rates of LHD w/o PH or PH-LHD SMCs. Analogously, although both control and LHD w/o PH SMCs had comparable proliferation rates at baseline, culturing these cells on the dECM produced by either LHD w/o PH or PH-LHD ECs increased Ki67⁺ SMCs relative to the baseline (Figure 3D). While neither dECM showed an additional effect on already hyperproliferative PH-LHD SMCs, PH-LHD SMCs cultured on a control dECM showed a decrease in proliferation rate relative to baseline (Figure 3D and E). These results suggest that the remodelled, yet not the naïve endothelial ECM promotes proliferation and migration of control SMCs, while a control endothelial ECM decreases the proliferation of PH-LHD SMCs. Consistent with a potential regulation of SMC dynamics by the ECM, we next demonstrated that the rate of SMC proliferation is sensitive to matrix stiffness, with control SMCs cultured on a collagen I matrix with a stiffness of 0.2 kPa (corresponding to ECM stiffness in controls) proliferating minimally, while SMCs proliferated rapidly on a stiffer ECM of 0.5 or 1 kPa (reflecting ECM stiffness in LHD w/o PH or PH-LHD patients, respectively) (Figure 3F and G). As such, the remodelled EC-derived ECM of LHD and particularly PH-LHD patients promotes the proliferation and migration of SMCs, thus potentially contributing to SMC hyperplasia and distal vessel muscularization in PH-LHD PAs.

3.4 YAP1 promotes SMC migration and proliferation in LHD w/o PH and PH-LHD

We next aimed to elucidate the mechanosensitive signalling mechanism by which SMCs respond to a remodelled or stiffer ECM. Mechanical cues from the cellular environment regulate TEAD-domain transcription factors through nuclear translocation of YAP1, a mechanosensitive co-activator within the Hippo signalling pathway.^{20,23,25,53} In PAH, YAP1 activation has been linked to ECM stiffening and the associated hyperproliferation of pulmonary vascular cells.^{23,44,54} Our previous work further demonstrated that activation of TAZ, a YAP1 homologue, promotes vascular calcification in SMCs in the context of PH-LHD,⁴⁷ providing a strong overall

rationale for the implication of the Hippo signalling pathway in lung vascular remodelling. As existing literature implicates YAP1 rather than TAZ as a key driver of SMC proliferation and migration in the context of neointima formation,^{55–59} we focused our further analyses on YAP1 activation in response to matrix stiffening.

We found that YAP1 nuclear abundance increases as a function of stiffness in control PA SMCs cultured on collagen 1 matrices of either 0.2, 0.5, or 1 kPa stiffness (Figure 4A and B). Importantly, a similar increase in nuclear YAP1 was detected in LHD w/o PH and PH-LHD SMCs relative to control SMCs when cultured on gelatin, indicating that SMC mechanosensitive signalling had been previously activated by mechanical cues in these patients (Figure 4C and D).

Given the established role of YAP1 as a regulator of physiological and neoplastic cell migration⁶⁰ and cell proliferation,^{61,62} we addressed the effect of functional YAP1 loss on these responses in PA SMCs. Loss of YAP1 function in SMCs was achieved either pharmacologically by treatment with VP or epigenetically by transfection with YAP1-targeting short interfering RNA (siYAP1), with YAP1 loss validated as reduced nuclear YAP1 abundance (Figure 4E and F). Both pharmacological inhibition and siRNA-mediated silencing of YAP1 significantly decreased SMC migration and proliferation rates in control, LHD w/o PH, and PH-LHD SMCs (Figure 4G–J; Supplementary material online, Figure S5), indicating that increased YAP1 activity may indeed drive SMC hyperplasia in PH-LHD.

3.5 Remodelled endothelial ECM regulates SMC migration and proliferation via YAP1 in LHD w/o PH and PH-LHD

Next, we tested whether YAP1 activation in LHD w/o PH and PH-LHD PA SMC may be attributed to endothelial ECM remodelling. Indeed, culturing on an dECM produced by ECs of LHD w/o PH and PH-LHD patients increased nuclear YAP1 abundance in control SMCs relative to culture on gelatin (baseline), yet had little additional effect on YAP1 activation in PH-LHD SMCs (Figure 5A–C, for experimental scheme please see Figure 3A). Conversely, culturing LHD w/o PH or PH-LHD SMCs on control dECM decreased their nuclear YAP1 levels relative to culture on gelatin (Figure 5C). These results emphasize the significance of the endothelial ECM in regulating YAP1 activation in PA SMCs.

Given that the dECM produced by ECs from LHD w/o PH or PH-LHD patients could by itself promote migration and proliferation of control SMC, we next addressed whether YAP1 inhibition by VP treatment could abolish these effects. As described above, the efficiency of YAP1 inhibition was confirmed by a quantitative reduction in nuclear YAP1 (Figure 5C). At the functional level, VP treatment reduced migration of control, LHD w/o PH, and PH-LHD SMCs across all culturing conditions, yet without reaching significance for PH-LHD SMCs cultured on a control endothelial dECM (Figure 5D; Supplementary material online, Figure S6). Analogous results were obtained for cell proliferation (Figure 5E; Supplementary material online, Figure S6). Notably, the effect of YAP1 inhibition on migration and proliferation of PH-LHD SMCs was comparable to the effect of culturing PH-LHD SMCs on a control endothelial dECM.

These data cumulatively demonstrate that remodelling and stiffening of the endothelial ECM in LHD w/o PH and PH-LHD PAs can promote the migration and proliferation of SMCs via YAP1-mediated mechanosensation. Hence, YAP1 emerges as an important downstream effector of endothelial ECM remodelling that may be targeted therapeutically to inhibit SMC hyperplasia in PH-LHD.

3.6 YAP1 inhibition attenuates PA SMC proliferation and migration in PH-LHD rats

To probe for a potential therapeutic effect of YAP1 inhibition on LHD-related PA SMC hyperplasia *in vivo*, we reprocessed biomaterials obtained from PH-LHD rats from a recent study by our lab.⁴⁷ In this study, PH-LHD was surgically induced by supracoronary AoB⁴⁶ and the treatment effect of the YAP1 inhibitor VP on pulmonary vascular calcification was examined. As demonstrated in this work, treatment with VP could

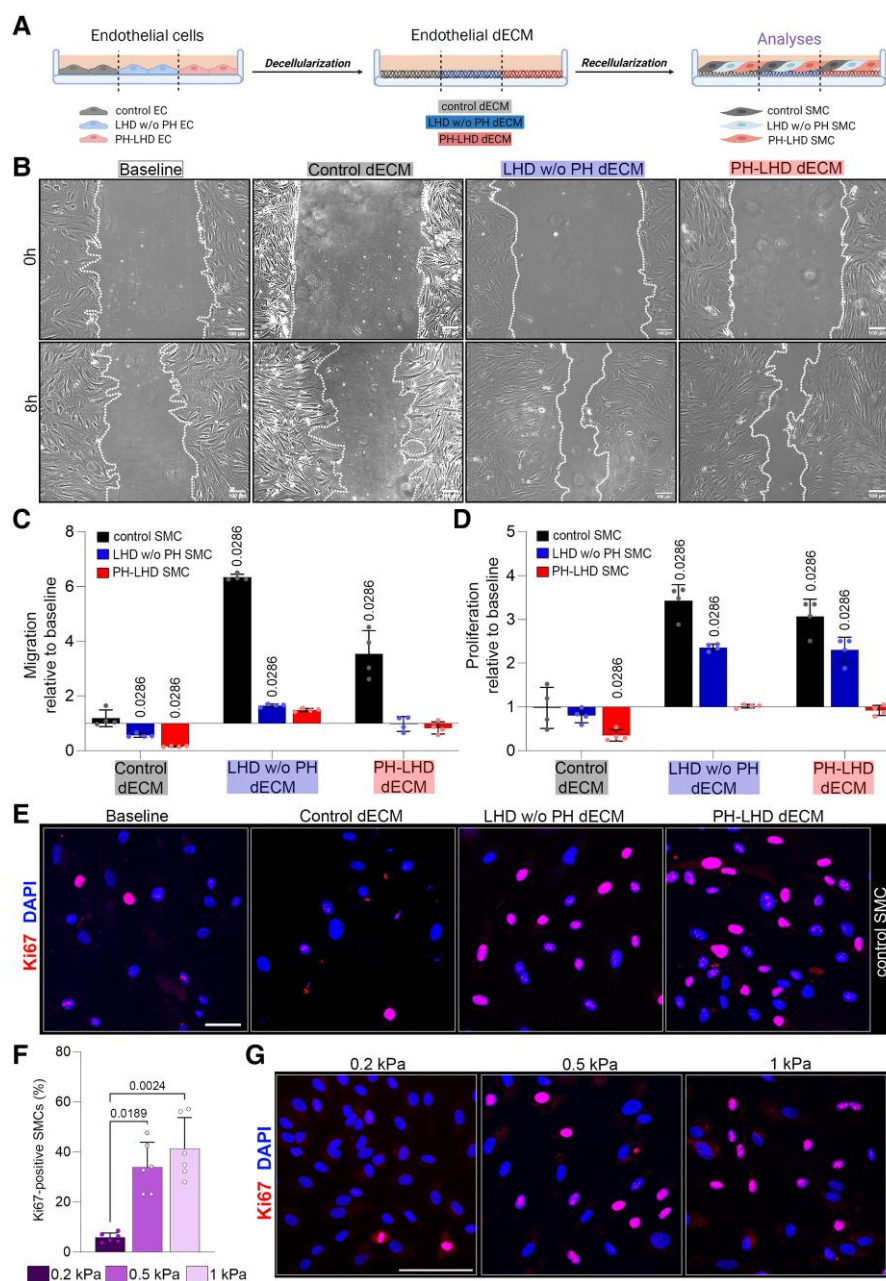


Figure 3 In LHD, a remodelled and stiffened endothelial ECM promotes SMC migration and proliferation. **A**, Schematic shows experimental setup for production of endothelial ECM, followed by EC decellularization (dECM) and recellularization by SMCs for *in vitro* analyses of SMC migration and proliferation as a function of endothelial ECM. **B**, Representative images of wound-healing assay performed on control SMCs cultured on dECM produced by ECs isolated from PAs of control subjects or LHD w/o PH or PH-LHD patients. Images taken at 0 and 8 h after scratching. **C**, Bar graph (mean + SD) with individual data points shows migration rate of SMCs isolated from PAs of control subjects ($n = 4$) and LHD w/o PH ($n = 4$) or PH-LHD ($n = 4$) patients cultured on dECM produced by ECs isolated from control, LHD w/o PH, or PH-LHD subjects. Migration rate is normalized to respective baseline (defined as migration rate on 0.1% gelatin). **D**, Bar graph (mean + SD) with individual data points shows proliferation rate of SMCs isolated from PAs of control subjects ($n = 4$), LHD w/o PH ($n = 4$), or PH-LHD ($n = 4$) patients cultured on dECM produced by ECs isolated from control, LHD w/o PH, or PH-LHD subjects. Proliferation rate is normalized to respective baseline (defined as proliferation rate on 0.1% gelatin). **E**, Respective confocal microscopic images show primary SMCs isolated from control subjects and cultured on dECM produced by ECs isolated from PAs of control subjects, LHD w/o PH, or PH-LHD patients and immunostained for the cell proliferation marker Ki67; nuclei are visualized by DAPI staining. **F**, Bar graph (mean + SD) with individual data points shows proliferation rate of SMCs isolated from PAs of control subjects and cultured on collagen I hydrogels with stiffness of either 0.2 kPa ($n = 6$ technical replicates), 0.5 kPa ($n = 6$ technical replicates), or 1 kPa ($n = 6$ technical replicates) corresponding to respective dECM stiffness produced by ECs isolated from PAs of control subjects and LHD w/o PH or PH-LHD patients. **G**, Representative confocal microscopic images show primary SMCs isolated from control subjects and cultured on collagen I hydrogels with stiffness of either 0.2, 0.5, or 1 kPa and immunostained for the cell proliferation marker Ki67; nuclei are visualized by DAPI staining. Scale bars are 100 μ m in **B**, 50 μ m in **E**, and 150 μ m in **G**. Statistics: Mann–Whitney *U* test (**C**, **D**) and Kruskal–Wallis test with Dunn’s correction for multiple comparisons in **F**; *P*-values for statistical significance are given.

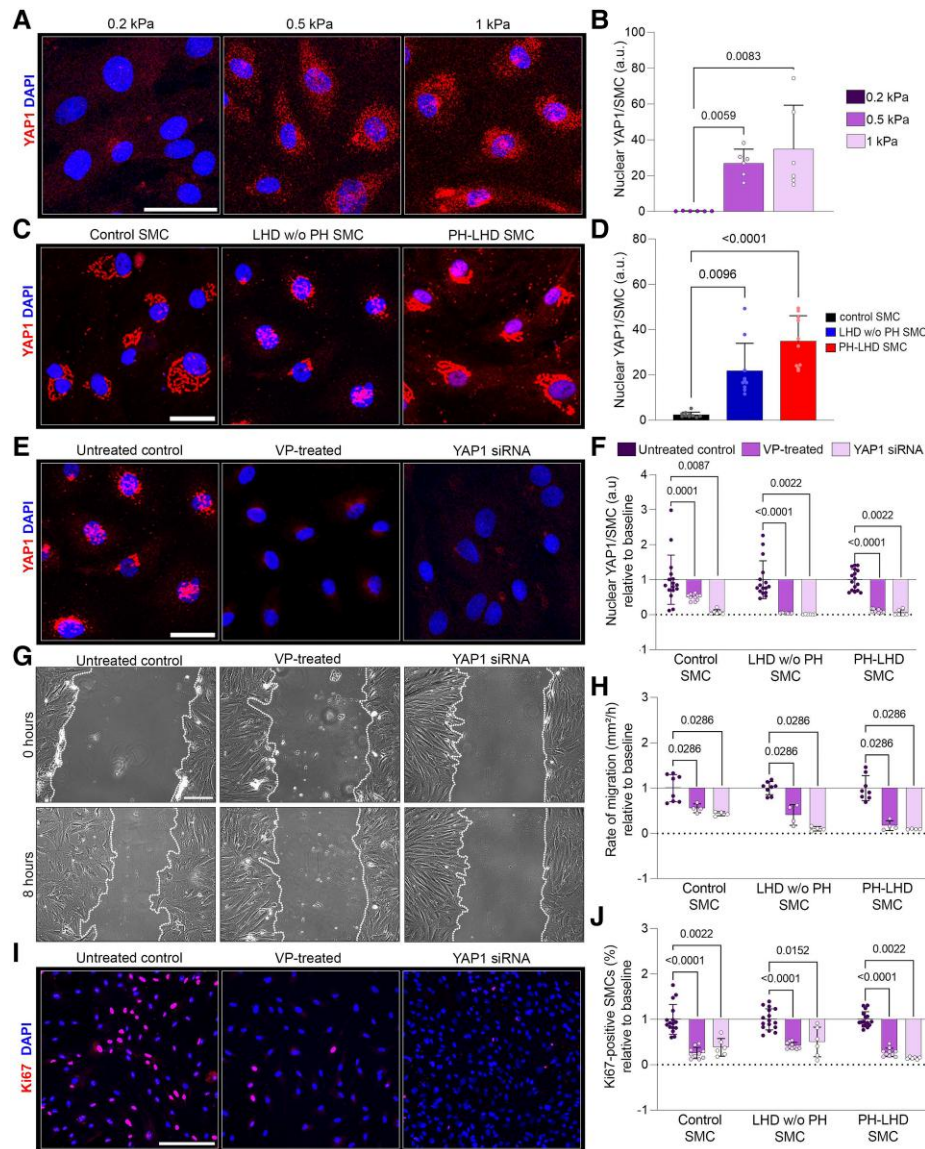


Figure 4 In LHD w/o PH, increased SMC migration and proliferation are regulated by YAP1. **A**, Representative confocal microscopic images show YAP1 immunostaining in SMCs isolated from PAs of control subjects and cultured on collagen I hydrogels of defined stiffnesses (0.2, 0.5, and 1 kPa); nuclei are visualized by DAPI staining. **B**, Bar graph (mean + SD) with individual data points shows quantification of nuclear YAP1 in SMCs isolated from PAs of control subjects and cultured on collagen I hydrogels of defined stiffnesses of 0.2 kPa ($n = 6$ technical replicates), 0.5 kPa ($n = 6$ technical replicates), and 1 kPa ($n = 6$ technical replicates). **C**, Representative confocal microscopic images show YAP1 immunostaining in SMCs isolated from PAs of control subjects and LHD w/o PH or PH-LHD patients and cultured on 0.1% gelatin; nuclei are visualized by DAPI staining. **D**, Bar graph (mean + SD) with individual data points shows quantification of nuclear YAP1 in SMCs isolated from PAs of control subjects ($n = 10$) and LHD w/o PH ($n = 10$) or PH-LHD ($n = 10$) patients and cultured on 0.1% gelatin. **E**, Representative confocal microscopic images show YAP1 immunostaining in SMCs isolated from PAs of LHD w/o PH subjects either prior to treatment (untreated control) or after YAP1 inhibition (VP or YAP1 siRNA); nuclei are visualized by DAPI staining. **F**, Bar graph (mean + SD) with individual data points shows quantification of nuclear YAP1 in SMCs isolated from PAs of control subjects ($n = 10$ for VP, $n = 6$ for siRNA YAP1) and LHD w/o PH ($n = 10$ for VP, $n = 6$ for siRNA YAP1) or PH-LHD ($n = 10$ for VP, $n = 6$ for siRNA YAP1) patients relative to corresponding untreated controls. **G**, Representative images of *in vitro* wound-healing assay performed on SMCs isolated from PAs of control subjects prior to treatment (untreated control) or after YAP1 inhibition (VP or YAP1 siRNA). Images taken at 0 and 8 h after scratching. **H**, Bar graph (mean + SD) with individual data points shows quantification of migration rates of SMCs isolated from PAs of control ($n = 4$) subjects and LHD w/o PH ($n = 4$) or PH-LHD ($n = 4$) patients after VP or YAP1 siRNA relative to untreated control (data sets were analysed in technical triplicates). **I**, Representative confocal microscopic images show Ki67 immunostaining in SMCs isolated from PAs of control subjects prior to treatment (untreated control) or after YAP1 inhibition (VP or YAP1 siRNA). **J**, Bar graph (mean + SD) with individual data points shows quantification of Ki67⁺ cells in SMCs isolated from PAs of control subjects ($n = 10$ for VP, $n = 6$ for siRNA YAP1) and LHD w/o PH ($n = 10$ for VP, $n = 6$ for siRNA YAP1) or PH-LHD ($n = 10$ for VP, $n = 6$ for siRNA YAP1) patients relative to untreated controls (data sets for untreated controls and VP-treated group were analysed in technical duplicates, data sets for siYAP1 knockdown were analysed in technical triplicates). Scale bars are 150 μ m in **A**, 50 μ m in **C**, and 100 μ m in **E**, **I**. Statistics: Kruskal–Wallis test with Dunn’s correction for multiple comparisons in **B** and **D**, and Mann–Whitney *U* test in **F**, **H**, and **J**; *P*-values for statistical significance are given.

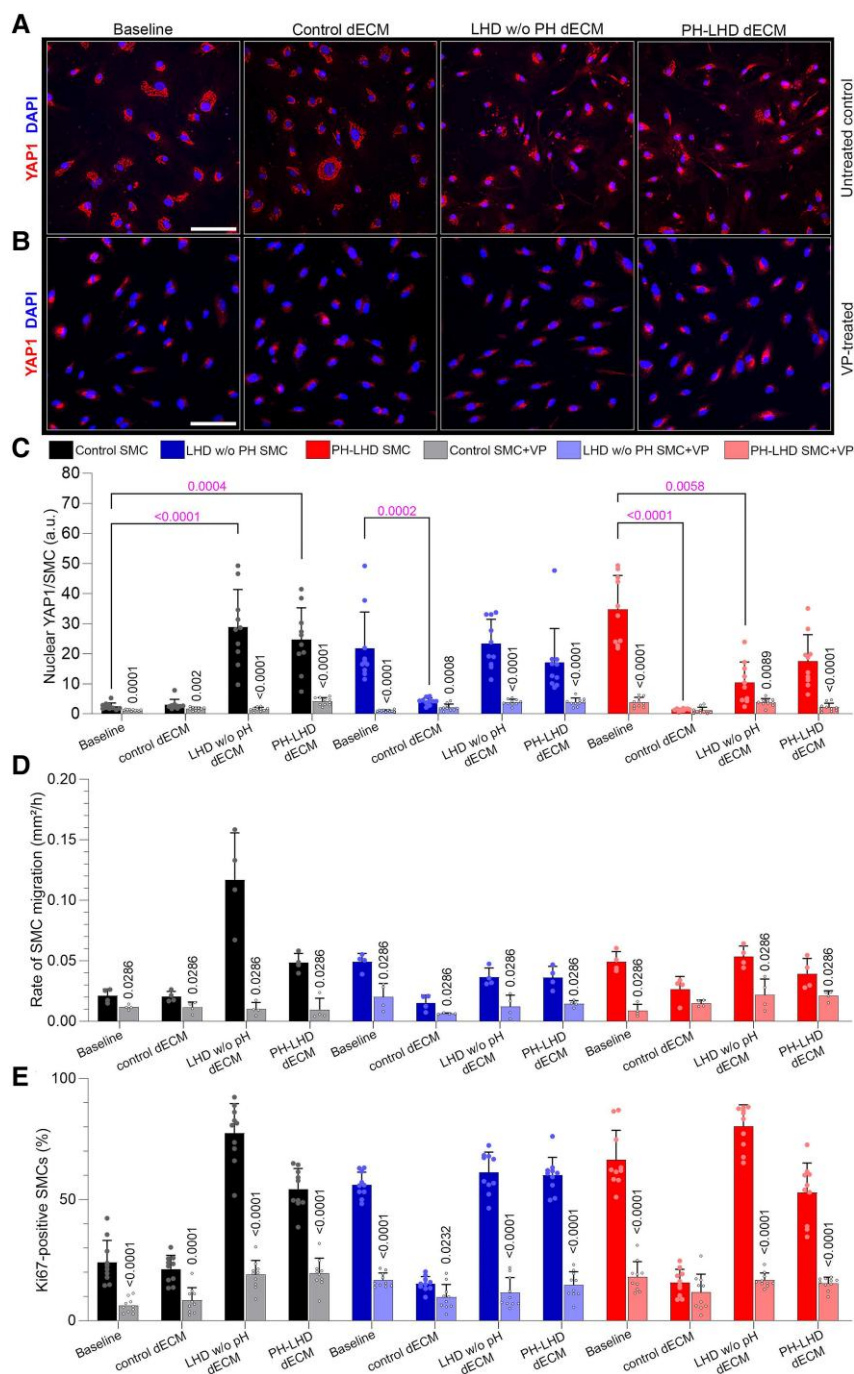


Figure 5 In LHD, the remodelled endothelial ECM regulates SMC function via YAP1. **A** and **B**, Representative confocal microscopic images show YAP1 immunostaining in SMCs isolated from PAs of control subjects and cultured on 0.1% gelatin (baseline), or on dECM produced by ECs isolated from control subjects and LHD w/o PH or PH-LHD patients in the absence (untreated) or presence of 1 mM VP; nuclei are visualized by DAPI staining. **C**, Bar graph (mean + SD) with individual data points shows quantification of nuclear YAP1 in SMCs isolated from PAs of control subjects ($n = 10$) and LHD w/o PH ($n = 10$) or PH-LHD ($n = 10$) patients cultured on either 0.1% gelatin (baseline) or on dECM produced by ECs isolated from PAs of control subjects and LHD w/o PH or PH-LHD patients in the absence (untreated) or presence of 1 mM VP (data sets were analysed as technical duplicates). **D**, Bar graph (mean + SD) with individual data points shows quantification of migration rates of SMCs isolated from PAs of control subjects ($n = 4$) and LHD w/o PH ($n = 4$) or PH-LHD ($n = 4$) patients and cultured on either 0.1% gelatin (baseline), or on dECM produced by ECs isolated from PAs of control subjects and LHD w/o PH or PH-LHD patients in the absence (untreated) or presence of 1 mM VP (data sets were analysed as technical triplicates). **E**, Bar graph (mean + SD) with individual data points shows quantification of Ki67⁺ nuclei in SMCs isolated from PAs of control subjects ($n = 10$) and LHD w/o PH ($n = 10$) or PH-LHD ($n = 10$) patients and culture on either 0.1% gelatin (baseline), or on dECM produced by ECs isolated from PAs of control subjects and LHD w/o PH or PH-LHD patients in the absence (untreated) or presence of 1 mM VP (data sets were analysed as technical duplicates). Scale bars are 50 μ m in **A** and **B**. Statistics: Kruskal–Wallis test with Dunn’s correction for multiple comparisons (**C**, in magenta), Mann–Whitney U test in (**C**, in black, **D**, **E**); P -values for statistical significance are given.

reverse PH in AoB rats, as evidenced by a decrease in right ventricular systolic pressure (RVSP) and right ventricular hypertrophy (see [online supplement Methods](#)). For the current study, we specifically examined the remodelling of the pulmonary arterial BM in AoB rats relative to sham-operated control rats and evaluated the effect of VP treatment on PA SMC proliferation and migration (for study scheme refer to [Supplementary material online, Figure S7](#)).

Microscopic analysis of the BM in rat PAs revealed that, compared to sham animals where COL4 appeared as a distinct thin line, the COL4 pattern in AoB animals showed both areas of widened and diminished signals, with the latter quantified as COL4 gaps ([Figure 6A and B](#)). BM remodelling in AoB rats mirrored the characteristics of BM remodelling observed in human PAs of both LHD w/o PH and PH-LHD patients. Specifically, primary SMCs isolated from PAs of AoB rats showed increased abundance of nuclear YAP1 relative to SMCs from PAs of sham rats ([Figure 6C and F](#)). *In vivo* treatment of AoB rats with VP reduced nuclear YAP1 levels in SMCs ([Figure 6C and G](#)). VP treatment also significantly decreased migration of SMCs from AoB rats compared to vehicle-treated controls ([Figure 6D, H, and I](#)). Although SMC proliferation was not significantly different between VP- and vehicle-treated AoB groups ($P = 0.7$), VP treatment attenuated proliferation to levels that were not significantly different from those observed in SMC from sham-operated controls ([Figure 6E, J, and K](#)).

Thus, we show that characteristics of human PA SMCs in LHD w/o PH and/or PH-LHD patients, such as activation of YAP1 and increased PA SMC migration and proliferation, could be replicated in PH-LHD rats but were attenuated by *in vivo* VP treatment. These results further indicate that the beneficial effect of VP treatment on PH in AoB rats could, at least in part, be attributable to reduced SMC hyperplasia and lung vascular remodelling.

4. Discussion

In this study, we identify the communication between a remodelled endothelial ECM and SMCs as a novel pathomechanism underlying PA SMC hyperplasia in PH-LHD. Our findings demonstrate that remodelling of the BM and stiffening of the endothelial ECM is present in patients with LHD w/o PH and PH-LHD, subsequently triggering YAP1 activation in SMCs and promoting their migration and proliferation. Conversely, the hyperproliferative and hypermigratory phenotype observed in PA SMCs from PH-LHD patients can be reversed when cells are cultured on a healthy endothelial ECM or treated with YAP1 inhibition ([Figure 7](#)). *In vivo*, YAP1 inhibition reduces PA SMC migration and proliferation and improves pulmonary haemodynamics in a rat model of PH-LHD. Thus, preserving or restoring a healthy ECM, as well as targeting YAP1, may offer promising therapeutic strategies to prevent or reverse SMC hyperplasia.

4.1 Vascular endothelial BM

In a healthy vascular bed, the endothelial BM provides an adhesive microenvironment crucial for maintaining the quiescence of the EC monolayer.⁶³ Beyond serving as an anchorage site for ECs, the endothelial BM forms a physical barrier regulating the transport of fluids, proteins, pharmaceuticals, and immune cells.^{32,64,65} Recently, the BM has also been recognized for its complex biomechanical properties, which may influence the phenotype of adjacent cells through mechanosensitive signalling pathways. Elastic modulus measurements of the BM using micropipette aspiration, glass cantilever systems, or AFM have revealed considerable variability in BM biomechanics, with stiffness ranging from 0.5 kPa to 5 MPa across different tissues and species.⁶⁶ However, the stiffness of the vascular endothelial BM and its modulation in cardiovascular pathologies remains poorly understood. Notably, BM stiffness may vary due to changes in protein composition, crosslinking, or the content of heparan sulfate proteoglycans, which regulate the hydration state of BMs.^{67,68} For instance, increased abundance of the dynamic BM component Netrin 4 softens the BM,⁶⁹ while sulfilimine-mediated COL4 crosslinking increases BM stiffness.⁷⁰

In the current study, we observed distinct alterations in the architecture of the endothelial BM in PAs of LHD patients. Immunostaining for COL4

and LAM, as well as TEM, revealed a significant widening of the BM in PAs of LHD w/o PH patients. This finding is consistent with previous reports of idiopathic PAH showing increased COL4 and LAM within a thickened endothelial BM.²⁵ Similarly, a marked widening of the BM at the alveolo-capillary barrier has been reported in a guinea pig model of LHD following AoB.⁷¹ In PAs of PH-LHD patients we had further detected signs of BM degradation which may reflect disease progression from LHD w/o PH to PH-LHD. Yet, this concept remains speculative as it could not be addressed within the limitations of the present cross-sectional study. Signs of both BM thickening and degradation, evident as BM gaps, were similarly observed in a rat model of PH-LHD.

AFM-based assessment of the biomechanical properties of dECM generated by PA ECs from healthy donors or LHD patients revealed an increase in stiffness from ~0.3 kPa for healthy to 0.5 kPa for LHD w/o PH and to 0.8 kPa for PH-LHD. In parallel, mass spectrometric analyses identified that both LHD w/o PH and PH-LHD ECs deposit more fibrillar collagens relative to control ECs with the highest abundances in LHD w/o PH. This seeming discrepancy between collagen abundance and matrix stiffness highlights the complexity of ECM remodelling that involves not only changes in protein quantities but other processes that determine mechanical properties such as intra- and inter-molecular crosslinking between fibrils. Collagen crosslinking increases ECM stiffness substantially and is primarily catalysed by lysyl oxidases (LOX) and transglutaminases (TG).¹⁸ Accordingly, elevated activity of LOX and/or TG2 has been associated with pronounced vascular stiffening and fibrosis in PH and fibrotic lung disease.^{72–74} Recent studies from our group have further demonstrated the accumulation of advanced glycation end products in the PA wall of LHD patients,²⁷ which may further promote collagen crosslinking. Increased ECM mineralization, as observed in PH-LHD,⁴⁷ also likely contributes to altered matrix mechanics.

4.2 PH-LHD associated changes in the endothelial-derived ECM promote SMC hyperplasia via activation of YAP1

In healthy PAs, SMCs are located apart from the endothelial BM. However, in PAs of LHD patients, SMCs tend to colocalize with the remodelled BM. This colocalization is associated with SMC hyperplasia and marked thickening of the PA wall, suggesting that BM remodelling may promote SMC proliferation and migration in LHD. This concept aligns with previous studies linking changes in BM composition and stiffness to distinct responses in BM-adjacent cells. BM stiffness, for example, has been shown to regulate the shape and the motility of juxtaposed cells thereby determining macroscopic shape during organ development.^{68,75–77} Similarly, BM stiffening in cancers due to loss of Netrin 4 promotes metastasis,^{78,79} while increased abundance of Nidogen 2 in the BM inhibits calcification in aortic SMC.⁸⁰

Of late, Hippo signalling has emerged as a major pathway by which cells sense the biomechanical context of their respective microenvironment.⁸¹ Consistently, we observed increased nuclear abundance of the Hippo pathway transcriptional co-activator YAP1 in SMCs of LHD patients, leading us to hypothesize that the remodelled and stiffened endothelial ECM induces SMC migration and/or proliferation via mechanosensitive Hippo signalling, ultimately resulting in SMC hyperplasia. YAP1 activation in PA SMCs has previously been implicated in PA remodelling in PAH,^{82,83} yet its role in PH-LHD and its relationship to BM remodelling have not been addressed. In subsequent experiments, we established a mechanistic link between endothelial ECM remodelling and stiffening and SMC migration and proliferation via YAP1 activation. Specifically, we show that (i) dECM produced by ECs of LHD w/o PH and PH-LHD patients activates YAP1 and concomitantly promotes migration and proliferation of healthy and LHD w/o PH SMCs, while (ii) dECM produced by ECs of healthy donors reduces YAP1 activation and normalizes migration and proliferation rates in PH-LHD SMCs; (iii) the effects summarized in (i) could be replicated by culturing SMC on stiffer matrices, yet (iv) migration and proliferation of SMCs derived from healthy, LHD w/o PH, or PH-LHD patients cultured on dECM produced by ECs from LHD w/o PH or PH-LHD patients

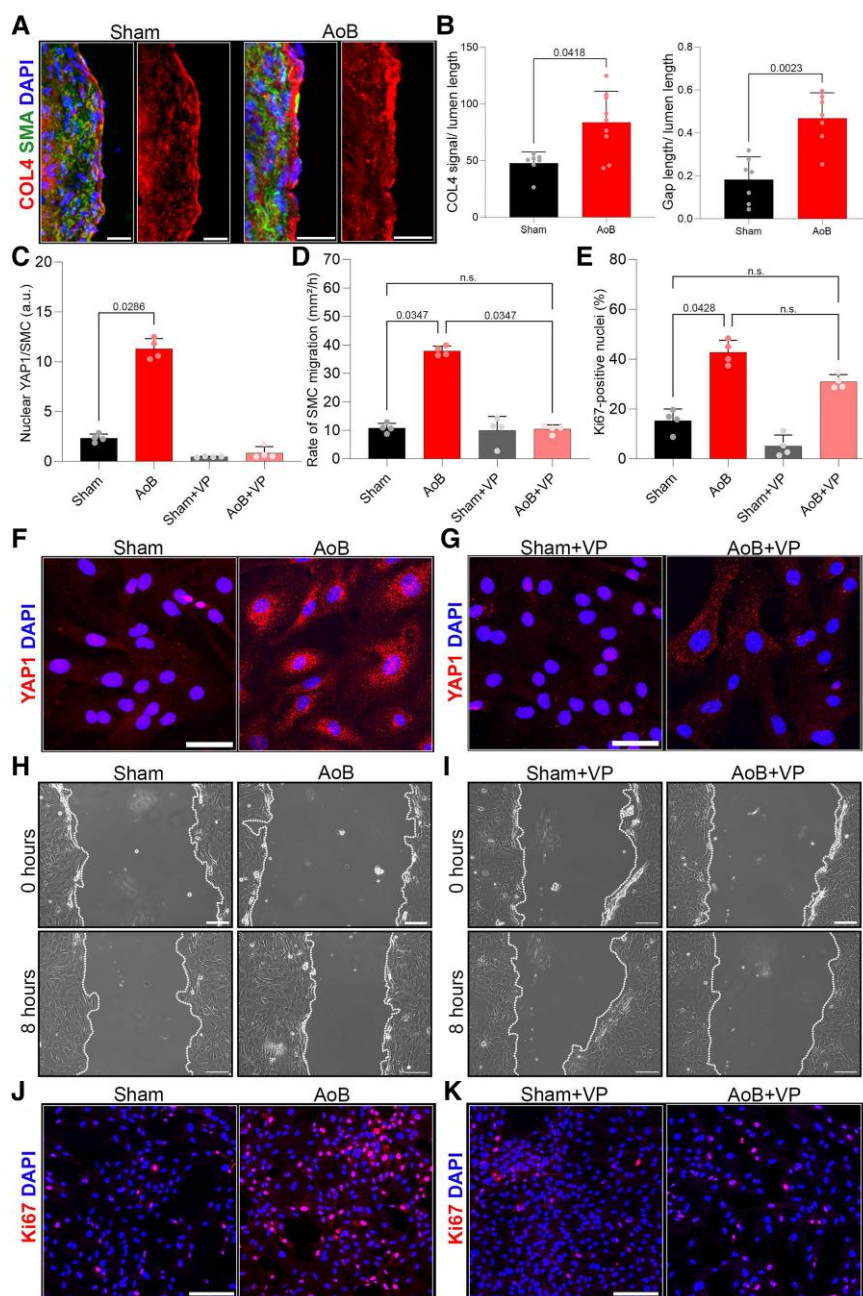
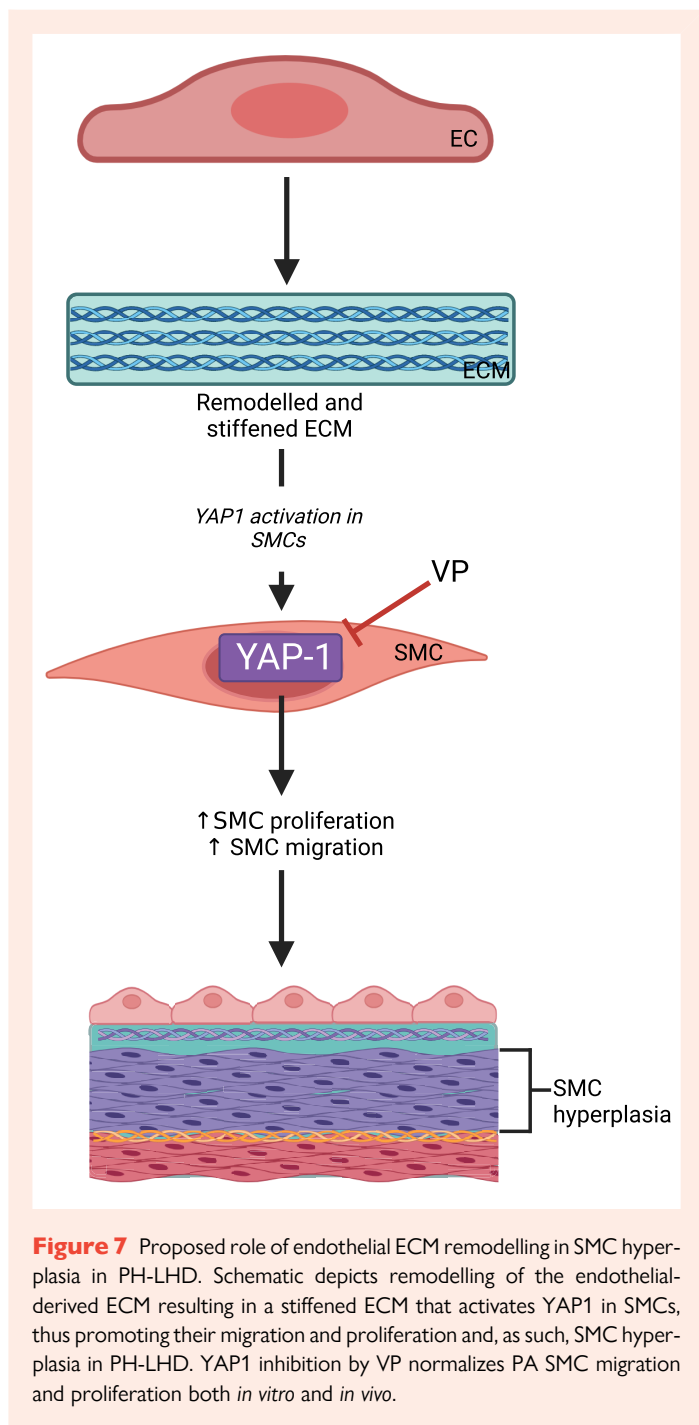


Figure 6 YAP1 inhibition attenuates SMC proliferation and migration in PH-LHD. **A**, Representative confocal microscopic images show collagen IV (COL4) immunostaining in PAs of sham and AoB rats. SMCs are identified by immunostaining for α -smooth muscle actin (SMA); nuclei are visualized by DAPI staining. **B**, Bar graphs (mean + SD) show quantification of COL4-positive BM area, and length of COL4-negative gaps relative to the length of the vascular lumen in PA samples of sham ($n = 7$) and AoB ($n = 9$) rats. **C**, Bar graph (mean + SD) shows quantitative analysis of nuclear YAP1/SMC in primary PA SMCs isolated from sham rats ($n = 4$), AoB rats ($n = 4$), sham rats treated with VP (Sham + VP, $n = 4$), and AoB rats treated with VP (AoB + VP, $n = 4$), with corresponding representative images shown in panels **F** and **G**. **D** and **E**, Bar graphs (mean + SD) show *in vitro* wound-healing assay performed on PA SMCs isolated from sham rats ($n = 4$), AoB rats ($n = 4$), sham rats treated with VP (Sham + VP, $n = 4$), and AoB rats treated with VP (AoB + VP, $n = 4$) at 0 and 8 h after making a scratch, with quantitative analysis of the rate of cell migration, as well as quantitative analysis of Ki67⁺ nuclei in primary PA SMCs isolated from sham rats ($n = 4$), AoB rats ($n = 4$), sham rats treated with VP (Sham + VP, $n = 4$), and AoB rats treated with VP (AoB + VP, $n = 4$), respectively. **F** and **G**, Representative immunostaining for YAP1 in primary PA SMCs isolated from sham rats ($n = 4$), AoB rats ($n = 4$), sham rats treated with VP (Sham + VP, $n = 4$), and AoB rats treated with VP (AoB + VP, $n = 4$) with nuclei counterstained by DAPI. **H–I** Representative bright field microscopic images of *in vitro* wound-healing assay performed on PA SMCs isolated from sham rats ($n = 4$), AoB rats ($n = 4$), sham rats treated with VP (Sham + VP, $n = 4$), and AoB rats treated with VP (AoB + VP, $n = 4$) at 0 and 8 h after making a scratch. **J** and **K** Representative confocal microscopic images showing an immunostaining for Ki67 in primary PA SMCs isolated from sham rats ($n = 4$), AoB rats ($n = 4$), sham rats treated with VP (Sham + VP, $n = 4$), and AoB rats treated with VP (AoB + VP, $n = 4$) with nuclei counterstained by DAPI, respectively. Scale bars at 20 μ m (**A**), 50 μ m (**F** and **G**), and 150 μ m (**F**, **G**, **J**, and **K**), respectively. Statistics: Mann–Whitney *U* test (**B**), Kruskal–Wallis test with Dunn’s corrections for multiple comparisons (**C–E**); *P*-values for statistical significance are given; n.s., not significant.



were normalized by YAP1 inhibition. Collectively, these findings demonstrate that PA ECs in LHD produce an altered, stiffened ECM that promotes SMC migration and proliferation via YAP1 activation. This signalling pathway may represent an important novel pathomechanism by which changes in the endothelial-derived ECM drive PA SMC hyperplasia in PH-LHD.

It is important to recognize that in response to matrix stiffening and/or hemodynamic changes characteristic of PH-LHD, multiple mechanosensitive signalling pathways may be activated—either in parallel, sequentially, or synergistically—and contribute to pulmonary vascular remodelling. In addition to YAP1, several other mechanotransducers have been implicated by us and others in related vascular pathologies and may be similarly relevant in PH-LHD including Piezo1,⁸⁴ Twist1,⁸⁵ or myocardin-related transcription factor A (MRTF-A).⁸⁶ As such, it is to be expected that the mechanosensitive landscape in PH-LHD is complex and involves multiple

interconnected pathways that drive vascular remodelling in response to the altered mechanical environment in PH-LHD.

Another important consideration relates to the substantial spatial heterogeneity of both vascular cell phenotypes and PH-LHD related changes in biomechanics (including e.g. ECM remodelling and stiffening, pulsatile pressure, and shear stress) along the length of the pulmonary arterial tree. For example in PH-LHD, the BM becomes excessively fibrotic and stiffened in proximal PAs, yet fragmented and leaky in distal arteries.⁸⁷ Similarly, ECs and SMCs exhibit significant phenotypic diversity along the PA tree and spatial borders between these phenotypes undergo further shifts in PH.⁸⁸ Spatial heterogeneity also applies to mechanical forces, with proximal PAs experiencing higher pulse pressures distal vessels more variable shear stresses. As a result of these spatial heterogeneities, caution is warranted when extrapolating findings from main conduit PAs to the more distal pulmonary vasculature.

Finally, we probed for the emerging recognition of YAP1 as a potential therapeutic target to counteract PA SMC hyperplasia in PH-LHD in a pre-clinical rat model of AoB-induced PH-LHD. This model replicates the features of endothelial BM remodelling observed in human LHD PAs, including YAP1 activation and increased SMC migration and proliferation. Treatment with VP mitigated several of these pathological features. Specifically, VP reduced nuclear YAP1 levels in SMCs from AoB rats and attenuated their enhanced migratory capacity to a level similar to the sham-vehicle group. Given that VP is already clinically approved as a photosensitizer for abnormal retinal vessels (e.g. in macular degeneration), it may represent a potent and readily implementable therapeutic strategy for the prevention or treatment of PH in LHD patients.

4.3 Study limitations

This study has several limitations that should be considered. First, the analysis of human PA tissue was limited to specimens from the PA trunk, as this is the only vascular tissue that can be routinely harvested during heart transplantation. Consequently, all human and rat pulmonary vascular cells used in this study were isolated from the main PA. While this approach ensures consistency and accessibility of vascular cell sources, it does not fully capture the cellular and structural heterogeneity, nor the potential differences in mechanical stimuli along the pulmonary arterial tree. Therefore, our findings should be interpreted with the understanding that the magnitude or nature of pulmonary vascular remodelling in the main PA may differ from processes in the distal PAs.

Second, while our data indicate that ECs from LHD w/o PH and, to a greater extent, PH-LHD patients deposit an ECM with increased stiffness and enriched with fibrillar collagens, these results should be interpreted with caution. *In vitro*-produced ECM may not fully reflect the *in vivo* BM topography, as BM remodelling, particularly degradation, in PH-LHD may also be influenced by other vascular cell types.

Third, the cross-sectional design of our study does not allow for definitive conclusions regarding the temporal sequence of pathological events in the development of PH-LHD. While observed phenotypes, such as BM remodelling, dECM stiffening, altered SMC functions, and intimal hyperplasia may indicate a sequential progression of pathological remodelling from LHD w/o PH to PH-LHD, this hypothesis requires confirmation by longitudinal studies.

Fourth, our work focused on elucidating the communication between an altered endothelial ECM and adjacent SMCs, while the specific pathomechanisms underlying BM remodelling in LHD remain to be fully understood. Lastly, we highlight ECM stiffening as a cause for YAP1 activation and subsequent SMC responses; however, additional biochemical signals, such as bioactive ECM degradation products (matrikines)⁸ or other secreted factors, may also contribute or synergistically interact with biomechanical effects in ECM-to-SMC signalling. Analogously, mechanical stimuli acting upon the pulmonary vasculature in PH-LHD, such as increased pressure, altered shear stress, or ECM remodelling and stiffening may activate additional mechanosensitive signalling pathways that operate in parallel, sequentially, or synergistically with YAP1 to regulate pulmonary vascular remodelling. While we recognize the probable complexity of the

mechanosensitive landscape in PH-LHD, the detailed dissection of these pathways was beyond the scope of the present study.

Fifth, due to sex-specific differences in growth rate, AoB results in different rates of aortic constriction in male and female rats, leading to divergent PH-LHD phenotypes over time as described in the Methods section. Within the current experimental framework, the female model could hence not be used for pharmacological intervention studies or for investigating potential sex-specific differences in PH-LHD.

Supplementary material

Supplementary material is available at [Cardiovascular Research](https://doi.org/10.1093/cvr/cvab011) online.

Authors' contributions

N.N.V., M.M.K., W.M.K., and C.K. conceived the clinical study and experimental design. N.N.V., T.G., A.A., M.K., S.-F.L. and M.M.K., performed experiments. F.H., R.Y., V.F., and C.K. performed surgeries and collected patient data and samples. R.S. provided methodology for the isolation of primary vascular cells. R.B.-H. developed image analysis software. N.N.V., M.K., P.M., R.S., M.W., V.F., M.M.K., W.M.K., and C.K. interpreted data. N.N.V., M.M.K., W.M.K., and C.K. supervised the study and wrote the manuscript. All authors reviewed, edited, and approved the manuscript. The authors M.M.K., W.M.K., C.K., and N.N.V. prepared and wrote the manuscript.

Acknowledgements

We thank Dr. Sara Timm, Petra Schrade, and Prof. Dr. Matthias Ochs of the Core Facility for Electron Microscopy of the Charité for their support in the acquisition of EM data, the Advanced Medical Bioimaging Core Facility (AMBIO) of the Charité for providing both the infrastructure and expertise for imaging and image analysis, Dr. Ansgar Petersen (Cellular BioMechanics and BioMaterials, Charité—Universitätsmedizin Berlin Julius Wolff Institute) for support with SHG imaging, and the operating room staff of the Deutsches Herzzentrum der Charité for their invaluable support in tissue collection.

Conflict of interest: none declared.

Funding

This study received support from the DZHK (German Centre for Cardiovascular Research) and the BMBF (German Federal Ministry of Education and Research) to C.K.; the Deutsche Forschungsgemeinschaft (SFB-TR84 A02 & C09, SFB1449 B01, SFB1470 A04, KU1218/11-1, and KU1218/12-1), the DZHK and the German Federal Ministry of Education and Research in the framework of SYMPATH (01ZX1906A) to W.M.K.; the Deutsche Stiftung für Herzforschung (DSHF, F/23/20 and F/58/23), the Deutsche Forschungsgemeinschaft (KU 4628/1-1), and the Sonnenfeld foundation (G05-24 and G09-25) to M.M.K.; the Deutsche Forschungsgemeinschaft (SFB1470 B05) to P.M.; and the DZHK and the German Cardiac Society (DGK) to N.N.V.

Data availability

The data underlying this article will be made available on reasonable request to the corresponding author.

References

1. Tsao CW, Aday AW, Almaraz ZI, Alonso A, Beaton AZ, Bittencourt MS, Boehme AK, Buxton AE, Carson AP, Commodore-Mensah Y, Elkind MSV, Evenson KR, Eze-Nliam C, Ferguson JF, Genesio G, Ho JE, Kalani R, Khan SS, Kissela BM, Knutson KL, Levine DA, Lewis TT, Liu J, Loop MS, Ma J, Mussolino ME, Navaneethan SD, Perak AM, Poudel R, Rezk-Hanna M, Roth GA, Schroeder EB, Shah SH, Thacker EL, VanWagner LB, Virani SS, Voecks JH, Wang NY, Yaffe K, Martin SS. Heart disease and stroke statistics-2022 update: a report from the American Heart Association. *Circulation* 2022;**145**:e153–e639.
2. Tiller D, Russ M, Greiser KH, Nuding S, Ebel H, Kluttig A, Kors JA, Thiery J, Bruegel M, Haerting J, Werdan K. Prevalence of symptomatic heart failure with reduced and with

- normal ejection fraction in an elderly general population—the CARLA study. *PLoS One* 2013;**8**:e59225.
3. Humbert M, Kovacs G, Hoepfer MM, Badagliacca R, Berger RMF, Brida M, Carlsen J, Coats AJS, Escribano-Subias P, Ferrari P, Ferreira DS, Ghofrani HA, Giannakoulas G, Kiely DG, Mayer E, Meszaros G, Nagavci B, Olsson KM, Pepke-Zaba J, Quint JK, Radegran G, Simonneau G, Sitbon O, Tonia T, Toshner M, Vachiery JL, Vonk Noordegraaf A, Delcroix M, Rosenkranz S; ESC/ERS Scientific Document Group. 2022 ESC/ERS guidelines for the diagnosis and treatment of pulmonary hypertension. *Eur Respir J* 2022;**61**:2200879.
4. Galie N, Humbert M, Vachiery JL, Gibbs S, Lang I, Torbicki A, Simonneau G, Peacock A, Vonk Noordegraaf A, Beghetti M, Ghofrani A, Gomez Sanchez MA, Hansmann G, Klepetko W, Lancellotti P, Matucci M, McDonagh T, Pierard LA, Trindade PT, Zompatori M, Hoepfer M. 2015 ESC/ERS guidelines for the diagnosis and treatment of pulmonary hypertension. *Rev Esp Cardiol (Engl Ed)* 2016;**69**:177.
5. Macera F, Vachiery JL. Management of pulmonary hypertension in left heart disease. *Methodist Debakey Cardiovasc J* 2021;**17**:115–123.
6. Crnkovic S, Marsh LM, El Agha E, Voswinckel R, Ghanim B, Klepetko W, Stacher-Priehe E, Olschewski H, Bloch W, Belluscio S, Olschewski A, Kwapiszewska G. Resident cell lineages are preserved in pulmonary vascular remodeling. *J Pathol* 2018;**244**:485–498.
7. Crnkovic S, Valzano F, Fliesser E, Gindlhuber J, Thekkarak Puthenparampil H, Basil M, Morley MP, Katzen J, Gschwandtner E, Klepetko W, Cantu E, Wolinski H, Olschewski H, Lindenmann J, Zhao YY, Morrissey EE, Marsh LM, Kwapiszewska G. Single-cell transcriptomics reveals skewed cellular communication and phenotypic shift in pulmonary artery remodeling. *JCI Insight* 2022;**7**:e153471.
8. Mutgan AC, Jandl K, Kwapiszewska G. Endothelial basement membrane components and their products, matrikines: active drivers of pulmonary hypertension? *Cells* 2020;**9**:2029.
9. Fayyaz AU, Edwards WD, Maleszewski JJ, Konik EA, DuBrock HM, Borlaug BA, Frantz RP, Jenkins SM, Redfield MM. Global pulmonary vascular remodeling in pulmonary hypertension associated with heart failure and preserved or reduced ejection fraction. *Circulation* 2018;**137**:1796–1810.
10. Shimoda LA, Laurie SS. Vascular remodeling in pulmonary hypertension. *J Mol Med (Berl)* 2013;**91**:297–309.
11. Olsson KM, Hoepfer MM, Pausch C, Grünig E, Huscher D, Pittrow D, Rosenkranz S, Gall H. Pulmonary vascular resistance predicts mortality in patients with pulmonary hypertension associated with interstitial lung disease: results from the COMPERA registry. *Eur Respir J* 2021;**58**:2101483.
12. Vanderpool RR, Kim AR, Molthen R, Chesler NC. Effects of acute Rho kinase inhibition on chronic hypoxia-induced changes in proximal and distal pulmonary arterial structure and function. *J Appl Physiol* (1985) 2011;**110**:188–198.
13. Yan D, Zhang D, Lu L, Qiu H, Wang J. Vascular endothelial growth factor-modified macrophages accelerate reendothelialization and attenuate neointima formation after arterial injury in atherosclerosis-prone mice. *J Cell Biochem* 2019;**120**:10652–10661.
14. Khan R, Agrotis A, Bobik A. Understanding the role of transforming growth factor-beta1 in intimal thickening after vascular injury. *Cardiovasc Res* 2007;**74**:223–234.
15. Lin CJ, Hunkins BM, Roth RA, Lin CY, Wagenseil JE, Mecham RP. Vascular smooth muscle cell subpopulations and neointimal formation in mouse models of elastin insufficiency. *Arterioscler Thromb Vasc Biol* 2021;**41**:2890–2905.
16. Kornowski R, Hong MK, Tio FO, Bramwell O, Wu H, Leon MB. In-stent restenosis: contributions of inflammatory responses and arterial injury to neointimal hyperplasia. *J Am Coll Cardiol* 1998;**31**:224–230.
17. Spiekeroetter E, Goncharova EA, Guignabert C, Stenmark K, Kwapiszewska G, Rabinovitch M, Voelkel N, Bogaard HJ, Graham B, Pullamsetti SS, Kuebler WM. Hot topics in the mechanisms of pulmonary arterial hypertension disease: cancer-like pathobiology, the role of the adventitia, systemic involvement, and right ventricular failure. *Pulm Circ* 2019;**9**:2045894019889775.
18. Thenappan T, Chan SY, Weir EK. Role of extracellular matrix in the pathogenesis of pulmonary arterial hypertension. *Am J Physiol Heart Circ Physiol* 2018;**315**:H1322–H1331.
19. Hoffmann J, Marsh LM, Pieper M, Stacher E, Ghanim B, Kovacs G, König P, Wilkens H, Haitchi HM, Hoefler G, Klepetko W, Olschewski H, Olschewski A, Kwapiszewska G. Compartment-specific expression of collagens and their processing enzymes in intrapulmonary arteries of IPAH patients. *Am J Physiol Lung Cell Mol Physiol* 2015;**308**:L1002–L1013.
20. Bertero T, Oldham WM, Cottrill KA, Pisano S, Vanderpool RR, Yu Q, Zhao J, Tai Y, Tang Y, Zhang YY, Rehman S, Sugahara M, Qi Z, Gorcsan J 3rd, Vargas SO, Saggarr R, Saggarr R, Wallace WD, Ross DJ, Haley KJ, Waxman AB, Parikh VN, De Marco T, Hsue PY, Morris A, Simon MA, Norris KA, Gaggioli C, Loscalzo J, Fessel J, Chan SY. Vascular stiffness mechanoregulates YAP/TAZ-dependent glutaminolysis to drive pulmonary hypertension. *J Clin Invest* 2016;**126**:3313–3335.
21. Chelladurai P, Seeger W, Pullamsetti SS. Matrix metalloproteinases and their inhibitors in pulmonary hypertension. *Eur Respir J* 2012;**40**:766–782.
22. Sun W, Chan SY. Pulmonary arterial stiffness: an early and pervasive driver of pulmonary arterial hypertension. *Front Med (Lausanne)* 2018;**5**:204.
23. Bertero T, Cottrill KA, Lu Y, Haeger CM, Dieffenbach P, Annis S, Hale A, Bhat B, Kaimal V, Zhang YY, Graham BB, Kumar R, Saggarr R, Saggarr R, Wallace WD, Ross DJ, Black SM, Fratz S, Fineman JR, Vargas SO, Haley KJ, Waxman AB, Chau BN, Fredenburgh LE, Chan SY. Matrix remodeling promotes pulmonary hypertension through feedback mechanoregulation of the YAP/TAZ-miR-130/301 circuit. *Cell Rep* 2015;**13**:1016–1032.
24. Ambade AS, Hassoun PM, Damico RL. Basement membrane extracellular matrix proteins in pulmonary vascular and right ventricular remodeling in pulmonary hypertension. *Am J Respir Cell Mol Biol* 2021;**65**:245–258.

25. Jandl K, Marsh LM, Hoffmann J, Mutgan AC, Baum O, Bloch W, Thekketkara-Puthenparampil H, Kolb D, Sinn K, Klepetko W, Heinemann A, Olschewski A, Olschewski H, Kwapiszewska G. Basement membrane remodeling controls endothelial function in idiopathic pulmonary arterial hypertension. *Am J Respir Cell Mol Biol* 2020;**63**:104–117.
26. Liu SF, Nambiar Veetil N, Li Q, Kucherenko MM, Knosalla C, Kuebler WM. Pulmonary hypertension: linking inflammation and pulmonary arterial stiffening. *Front Immunol* 2022;**13**:959209.
27. Kucherenko MM, Sang P, Yao J, Gransar T, Dhital S, Grune J, Simmons S, Michalick L, Wulsten D, Thiele M, Shomroni O, Hennig F, Yeter R, Solowjowa N, Salinas G, Duda GN, Falk V, Vyavahare NR, Kuebler WM, Knosalla C. Elastin stabilization prevents impaired biomechanics in human pulmonary arteries and pulmonary hypertension in rats with left heart disease. *Nat Commun* 2023;**14**:4416.
28. Hallmann R, Hannocks MJ, Song J, Zhang X, Di Russo J, Luik AL, Burmeister M, Gerwien H, Sorokin L. The role of basement membrane laminins in vascular function. *Int J Biochem Cell Biol* 2020;**127**:105823.
29. Li L, Song J, Chuquisana O, Hannocks MJ, Loismann S, Vogl T, Roth J, Hallmann R, Sorokin L. Endothelial basement membrane laminins as an environmental cue in monocyte differentiation to macrophages. *Front Immunol* 2020;**11**:584229.
30. Song J, Zhang X, Buscher K, Wang Y, Wang H, Di Russo J, Li L, Lütke-Enking S, Zarbock A, Stadtmann A, Striowski P, Wirth B, Kuzmanov I, Wiendl H, Schulte D, Vestweber D, Sorokin L. Endothelial basement membrane laminin 511 contributes to endothelial junctional tightness and thereby inhibits leukocyte transmigration. *Cell Rep* 2017;**18**:1256–1269.
31. Wu C, Ivars F, Anderson P, Hallmann R, Vestweber D, Nilsson P, Robenek H, Tryggvason K, Song J, Korpos E, Loser K, Beissert S, Georges-Labouesse E, Sorokin LM. Endothelial basement membrane laminin alpha5 selectively inhibits T lymphocyte extravasation into the brain. *Nat Med* 2009;**15**:519–527.
32. Zhang X, Wang Y, Song J, Gerwien H, Chuquisana O, Chashchina A, Denz C, Sorokin L. The endothelial basement membrane acts as a checkpoint for entry of pathogenic T cells into the brain. *J Exp Med* 2020;**217**:e20191339.
33. Hayden MR, Sowers JR, Tyagi SC. The central role of vascular extracellular matrix and basement membrane remodeling in metabolic syndrome and type 2 diabetes: the matrix pre-loaded. *Cardiovasc Diabetol* 2005;**4**:9.
34. Holm Nielsen S, Tengryd C, Edsfieldt A, Brix S, Genovese F, Bengtsson E, Karsdal M, Leeming DJ, Nilsson J, Gonçalves I. Markers of basement membrane remodeling are associated with higher mortality in patients with known atherosclerosis. *J Am Heart Assoc* 2018;**7**:e009193.
35. Rhodes CJ, Im H, Cao A, Hennigs JK, Wang L, Sa S, Chen PI, Nickel NP, Miyagawa K, Hopper RK, Tojais NF, Li CG, Gu M, Spiekerkoetter E, Xian Z, Chen R, Zhao M, Kaschwisch M, Del Rosario PA, Bernstein D, Zamanian RT, Wu JC, Snyder MP, Rabinovitch M. RNA sequencing analysis detection of a novel pathway of endothelial dysfunction in pulmonary arterial hypertension. *Am J Respir Crit Care Med* 2015;**192**:356–366.
36. Dasgupta I, McCollum D. Control of cellular responses to mechanical cues through YAP/TAZ regulation. *J Biol Chem* 2019;**294**:17693–17706.
37. Pietilä EA, Gonzalez-Molina J, Moyano-Galceran L, Jamalzadeh S, Zhang K, Lehtinen L, Turunen SP, Martins TA, Gultekin O, Lamminen T, Kaipio K, Joneborg U, Hynninen J, Hietanen S, Grénman S, Lehtonen R, Hautaniemi S, Carpen O, Carlson JW, Lehti K. Co-evolution of matrisome and adaptive adhesion dynamics drives ovarian cancer chemoresistance. *Nat Commun* 2021;**12**:3904.
38. Holland EN, Fernández-Yagüe MA, Zhou DW, O'Neill EB, Woodfolk AU, Mora-Boza A, Fu J, Schlaepfer DD, García AJ. FAK, vinculin, and talin control mechanosensitive YAP nuclear localization. *Biomaterials* 2024;**308**:122542.
39. Bart N, Hungerford S, Emmanuel S, Kotlyar E, Keogh A, MacDonald P, Muller D, Hayward C. Pre-operative pulmonary artery pulsatility index does not predict mortality post-cardiac transplantation. *ESC Heart Fail* 2023;**10**:1980–1986.
40. Bachmann KF, Moller PW, Hunziker L, Maggiorini M, Berger D. Mechanisms maintaining right ventricular contractility-to-pulmonary arterial elastance ratio in VA ECMO: a retrospective animal data analysis of RV-PA coupling. *J Intensive Care* 2024;**12**:19.
41. Driscoll TP, Cosgrove BD, Heo SJ, Shurden ZE, Mauck RL. Cytoskeletal to nuclear strain transfer regulates YAP signaling in mesenchymal stem cells. *Biophys J* 2015;**108**:2783–2793.
42. Elosgui-Artola A, Andreu I, Beedle AEM, Lezamiz A, Uroz M, Kosmalska AJ, Oria R, Kechagia JZ, Rico-Lastres P, Le Roux AL, Shanahan CM, Trepat X, Navajas D, Garcia-Manes S, Roca-Cusachs P. Force triggers YAP nuclear entry by regulating transport across nuclear pores. *Cell* 2017;**171**:1397–1410.e1314.
43. Kofler M, Kapus A. Nuclear import and export of YAP and TAZ. *Cancers (Basel)* 2023;**15**:4956.
44. Dieffenbach PB, Haeger CM, Coronata AMF, Choi KM, Varelas X, Tschumperlin DJ, Fredenburgh LE. Arterial stiffness induces remodeling phenotypes in pulmonary artery smooth muscle cells via YAP/TAZ-mediated repression of cyclooxygenase-2. *Am J Physiol Lung Cell Mol Physiol* 2017;**313**:L628–L647.
45. Hoffmann J, Yin J, Kukucka M, Yin N, Saarikko I, Sterner-Kock A, Fujii H, Leong-Poi H, Kuppe H, Schermuly RT, Kuebler WM. Mast cells promote lung vascular remodelling in pulmonary hypertension. *Eur Respir J* 2011;**37**:1400–1410.
46. Sang P, Kucherenko MM, Yao J, Li Q, Simmons S, Kuebler WM, Knosalla C. A model of reverse vascular remodeling in pulmonary hypertension due to left heart disease by aortic debanding in rats. *J Vis Exp* 2022;**181**. doi: 10.3791/63502.
47. Liu SF, Kucherenko MM, Sang P, Li Q, Yao J, Nambiar Veetil N, Gransar T, Alesutan I, Voelkl J, Salinas G, Grune J, Simmons S, Knosalla C, Kuebler WM. RUNX2 is stabilised by TAZ and drives pulmonary artery calcification and lung vascular remodelling in pulmonary hypertension due to left heart disease. *Eur Respir J* 2024;**64**:2300844.
48. Kucherenko MM, Kukucka M, Sang P, Hegemann N, Li Q, Hennig F, Yeter R, Gransar T, Mladenow A, Emmerich A, Orsenigo A, Grune J, Falk V, Kuebler WM, Knosalla C. Identification of pulmonary artery stiffening due to left heart disease by ultrasonography. *Cardiovasc Res* 2025;**121**:1433–1447.
49. Zaidel-Bar R, Ballestrem C, Kam Z, Geiger B. Early molecular events in the assembly of matrix adhesions at the leading edge of migrating cells. *J Cell Sci* 2003;**116**:4605–4613.
50. Deakin NO, Turner CE. Distinct roles for paxillin and Hic-5 in regulating breast cancer cell morphology, invasion, and metastasis. *Mol Biol Cell* 2011;**22**:327–341.
51. Carisey A, Tsang R, Greiner AM, Nijenhuis N, Heath N, Nazgiewicz A, Kemkemer R, Derby B, Spatz J, Ballestrem C. Vinculin regulates the recruitment and release of core focal adhesion proteins in a force-dependent manner. *Curr Biol* 2013;**23**:271–281.
52. Deakin NO, Turner CE. Paxillin comes of age. *J Cell Sci* 2008;**121**:2435–2444.
53. Yatsenko AS, Kucherenko MM, Xie Y, Aweida D, Urlaub H, Scheibe RJ, Cohen S, Shcherbata HR. Profiling of the muscle-specific dystroglycan interactome reveals the role of Hippo signaling in muscular dystrophy and age-dependent muscle atrophy. *BMC Med* 2020;**18**:8.
54. Dieffenbach PB, Maracle M, Tschumperlin DJ, Fredenburgh LE. Mechanobiological feedback in pulmonary vascular disease. *Front Physiol* 2018;**9**:51.
55. Dupont S, Morsut L, Aragona M, Enzo E, Giulitti S, Cordenonsi M, Zanconato F, Le Digele J, Forcato M, Bicciato S, Elvassore N, Piccolo S. Role of YAP/TAZ in mechanotransduction. *Nature* 2011;**474**:179–183.
56. Wang X, Hu G, Gao X, Wang Y, Zhang W, Harmon EY, Zhi X, Xu Z, Lennartz MR, Barroso M, Trebak M, Chen C, Zhou J. The induction of yes-associated protein expression after arterial injury is crucial for smooth muscle phenotypic modulation and neointima formation. *Arterioscler Thromb Vasc Biol* 2012;**32**:2662–2669.
57. Xu F, Ahmed AS, Kang X, Hu G, Liu F, Zhang W, Zhou J. MicroRNA-15b/16 attenuates vascular neointima formation by promoting the contractile phenotype of vascular smooth muscle through targeting YAP. *Arterioscler Thromb Vasc Biol* 2015;**35**:2145–2152.
58. Garoffolo G, Sluiter TJ, Thomas A, Piacentini L, Rutter MS, Schiavo A, Salvi M, Saccu C, Zoli S, Chiesa M, Yokoyama T, Agrifoglio M, Soncini M, Fiore GB, Martelli F, Condorelli G, Madeddu P, Molinari F, Morbiducci U, Quax PHA, Spinetti G, de Vries MR, Pesce M. Blockade of YAP mechanotransduction prevents neointima formation and adverse remodeling in arterialized vein grafts. *J Am Heart Assoc* 2025;**14**:e037531.
59. Osman I, Dong K, Kang X, Yu L, Xu F, Ahmed ASI, He X, Shen J, Hu G, Zhang W, Zhou J. YAP1/TEAD1 upregulate platelet-derived growth factor receptor beta to promote vascular smooth muscle cell proliferation and neointima formation. *J Mol Cell Cardiol* 2021;**156**:20–32.
60. Mason DE, Collins JM, Dawahare JH, Nguyen TD, Lin Y, Voytik-Harbin SL, Zorlutuna P, Yoder MC, Boerckel JD. YAP and TAZ limit cytoskeletal and focal adhesion maturation to enable persistent cell motility. *J Cell Biol* 2019;**218**:1369–1389.
61. Sun D, Li X, He Y, Li W, Wang Y, Wang H, Jiang S, Xin Y. YAP1 enhances cell proliferation, migration, and invasion of gastric cancer in vitro and in vivo. *Oncotarget* 2016;**7**:81062–81076.
62. Fu D, Lv X, Hua G, He C, Dong J, Lele SM, Li DW, Zhai Q, Davis JS, Wang C. YAP regulates cell proliferation, migration, and steroidogenesis in adult granulosa cell tumors. *Endocr Relat Cancer* 2014;**21**:297–310.
63. Lopera Higuaita M, Shortreed NA, Dasari S, Griffiths LG. Basement membrane of tissue engineered extracellular matrix scaffolds modulates rapid human endothelial cell recellularization and promote quiescent behavior after monolayer formation. *Front Bioeng Biotechnol* 2022;**10**:903907.
64. Morris AW, Sharp MM, Albargothy NJ, Fernandes R, Hawkes CA, Verma A, Weller RO, Carare RO. Vascular basement membranes as pathways for the passage of fluid into and out of the brain. *Acta Neuropathol* 2016;**131**:725–736.
65. Thomsen MS, Routhie LJ, Moos T. The vascular basement membrane in the healthy and pathological brain. *J Cereb Blood Flow Metab* 2017;**37**:3300–3317.
66. Leclech C, Natale CF, Barakat AL. The basement membrane as a structured surface—role in vascular health and disease. *J Cell Sci* 2020;**133**:jcs239889.
67. Candiello J, Cole GJ, Halfter W. Age-dependent changes in the structure, composition and biophysical properties of a human basement membrane. *Matrix Biol* 2010;**29**:402–410.
68. Pastor-Pareja JC, Xu T. Shaping cells and organs in Drosophila by opposing roles of fat body-secreted Collagen IV and perlecan. *Dev Cell* 2011;**21**:245–256.
69. Mehlen P, Fattet L, Netrin-4 regulates stiffness and metastasis. *Nat Mater* 2021;**20**:722–723.
70. Bhavé G, Colon S, Ferrell N. The sulfhydryl cross-link of collagen IV contributes to kidney tubular basement membrane stiffness. *Am J Physiol Renal Physiol* 2017;**313**:F596–F602.
71. Huang W, Kingsbury MP, Turner MA, Donnelly JL, Flores NA, Sheridan DJ. Capillary filtration is reduced in lungs adapted to chronic heart failure: morphological and haemodynamic correlates. *Cardiovasc Res* 2001;**49**:207–217.
72. Guo T, He C, Venado A, Zhou Y. Extracellular matrix stiffness in lung health and disease. *Compr Physiol* 2022;**12**:3523–3558.
73. Tjin G, White ES, Faiz A, Sicard D, Tschumperlin DJ, Mahar A, Kable EPW, Burgess JK. Lysyl oxidases regulate fibrillar collagen remodelling in idiopathic pulmonary fibrosis. *Dis Model Mech* 2017;**10**:1301–1312.
74. Nguyen XX, Nishimoto T, Takihara T, Mlakar L, Bradshaw AD, Feghali-Bostwick C. Lysyl oxidase directly contributes to extracellular matrix production and fibrosis in systemic sclerosis. *Am J Physiol Lung Cell Mol Physiol* 2021;**320**:L29–L40.
75. Crest J, Diz-Muñoz A, Chen DY, Fletcher DA, Bilder D. Organ sculpting by patterned extracellular matrix stiffness. *Elife* 2017;**6**:e24958.
76. Chlata J, Milani P, Runel G, Duteyrat JL, Arias L, Lamié LA, Boudaoud A, Grammont M. Variations in basement membrane mechanics are linked to epithelial morphogenesis. *Development* 2017;**144**:4350–4362.

77. Ramos-Lewis W, Page-McCaw A. Basement membrane mechanics shape development: lessons from the fly. *Matrix Biol* 2019;**75–76**:72–81.
78. Reuten R, Zendeheroud S, Nicolau M, Fleischhauer L, Laitala A, Kiderlen S, Nikodemus D, Wullkopf L, Nielsen SR, McNeilly S, Prein C, Rafeeva M, Schoof EM, Furtwängler B, Porse BT, Kim H, Wwon KJ, Sudhop S, Zornhagen KW, Suhr F, Maniati E, Pearce OMT, Koch M, Oddershede LB, Van Agtmael T, Madsen CD, Mayorca-Guiliani AE, Bloch W, Netz RR, Clausen-Schaumann H, Erler JT. Basement membrane stiffness determines metastases formation. *Nat Mater* 2021;**20**:892–903.
79. Liotta LA, Tryggvason K, Garbisa S, Hart I, Foltz CM, Shafie S. Metastatic potential correlates with enzymatic degradation of basement membrane collagen. *Nature* 1980;**284**: 67–68.
80. Chen Y, Mao C, Gu R, Zhao R, Li W, Ma Z, Jia Y, Yu F, Luo J, Fu Y, Sun J, Kong W. Nidogen-2 is a novel endogenous ligand of LGR4 to inhibit vascular calcification. *Circ Res* 2022;**131**: 1037–1054.
81. Panciera T, Azzolin L, Cordenonsi M, Piccolo S. Mechanobiology of YAP and TAZ in physiology and disease. *Nat Rev Mol Cell Biol* 2017;**18**:758–770.
82. Kudryashova TV, Goncharov DA, Pena A, Kelly N, Vanderpool R, Baust J, Kobir A, Shufesky W, Mora AL, Morelli AE, Zhao J, Ihida-Stansbury K, Chang B, DeLisser H, Tudor RM, Kawut SM, Silljé HH, Shapiro S, Zhao Y, Goncharova EA. HIPPO-Integrin-linked kinase cross-talk controls self-sustaining proliferation and survival in pulmonary hypertension. *Am J Respir Crit Care Med* 2016;**194**:866–877.
83. Zuo W, Liu N, Zeng Y, Xiao Z, Wu K, Yang F, Li B, Song Q, Xiao Y, Liu Q. Luteolin ameliorates experimental pulmonary arterial hypertension via suppressing hippo-YAP/PI3K/AKT signaling pathway. *Front Pharmacol* 2021;**12**:663551.
84. Lai A, Cox CD, Chandra Sekar N, Thurgood P, Jaworowski A, Peter K, Baratchi S. Mechanosensing by Piezo1 and its implications for physiology and various pathologies. *Biol Rev Camb Philos Soc* 2022;**97**:604–614.
85. Fan Y, Gu X, Zhang J, Sinn K, Klepetko W, Wu N, Foris V, Solymosi P, Kwapiszewska G, Kuebler WM. TWIST1 drives smooth muscle cell proliferation in pulmonary hypertension via loss of GATA-6 and BMPR2. *Am J Respir Crit Care Med* 2020;**202**:1283–1296.
86. Zabini D, Granton E, Hu Y, Miranda MZ, Weichelt U, Breuils Bonnet S, Bonnet S, Morrell NW, Connelly KA, Provencher S, Ghanim B, Klepetko W, Olschewski A, Kapus A, Kuebler WM. Loss of SMAD3 promotes vascular remodeling in pulmonary arterial hypertension via MRTF disinhibition. *Am J Respir Crit Care Med* 2018;**197**:244–260.
87. Mora Massad K, Dai Z, Petrache I, Ventetuolo CE, Lahm T. Lung endothelial cell heterogeneity in health and pulmonary vascular disease. *Am J Physiol Lung Cell Mol Physiol* 2025;**328**: L877–L884.
88. Zhang Q, Yaoita N, Tabuchi A, Liu S, Chen SH, Li Q, Hegemann N, Li C, Rodor J, Timm S, Laban H, Finkel T, Stevens T, Alvarez DF, Erfinanda L, de Perrot M, Kucherenko MM, Knosalla C, Ochs M, Dimmeler S, Korff T, Verma S, Baker AH, Kuebler WM. Endothelial heterogeneity in the response to autophagy drives small vessel muscularization in pulmonary hypertension. *Circulation* 2024;**150**:466–487.